Engineering Structures 289 (2023) 115812

Contents lists available at ScienceDirect

Engineering Structures

journal homepage: www.elsevier.com/locate/engstruct

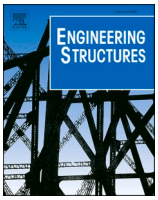

Characterizing wind-structure interaction for performance-based wind design of tall buildings

Smrithi Preetha Hareendran [a], Alice Alipour [a,*], Behrouz Shafei [a], Partha Sarkar [b]

[a] Department of Civil, Construction and Environmental Engineering, Iowa State University, Ames, IA, United States
[b] Department of Aerospace Engineering, Iowa State University, Ames, IA, United States

ARTICLE INFO

Keywords:
Performance-based design
Tall buildings
Wind-loads
Self-excited forces
Nonlinearity
Interaction parameter

ABSTRACT

Performance-based wind design (PBWD) has been receiving a great deal of attention from the wind and structural engineering communities. This is specifically highlighted with the release of the ASCE pre-standard for PBWD (2019). The PBWD of tall building requires a series of steps one of which is the interaction parameter, i.e. characterizing the interaction of the tall building with the wind field. In the studies involving slender structures-such as tall buildings, it is essential to consider this interaction parameter which is a function of the time-varying aerodynamic loads. The aerodynamic loads consist of the turbulent loads due to fluctuating wind, known as buffeting loads, and the self-excited loads resulting from the interaction of the structural motions with wind, referred as aeroelastic loads. Flexible structures can become unstable at a critical wind speed, known as flutter speed, wherein a diverging motion of the structure occurs. Aerodynamic instability that is caused by self-excited loads generally doesn't occur in tall buildings within their design wind speeds but certainly needs to be considered in a wind-structure interaction analysis, particularly when tall buildings become increasingly slender and are allowed to enter post-elastic region. This study aims to characterize the interaction parameter in the PBWD of tall buildings by including the self-excited loads in its response analysis corresponding to the three-degree-of-freedom response motions of the building in along-wind, across-wind, and torsional directions. For this purpose, the flutter derivatives that are used to represent the self-excited loads in frequency domain are first obtained from wind tunnel tests of scaled section models of the structure and then converted into approximate coefficients known as Rational Function Coefficients (RFC) as part of Rational Function Approximations (RFA) of the self-excited loads in Laplace or time domain. The wind loads on a structure in time domain are calculated by combining both the buffeting loads and self-excited loads associated with the calculated RFC. The non-linear structural behavior of a 44-story and a 60-story tall building each is studied using nonlinear dynamic time-history analysis in extreme wind conditions and then observed for any flutter-like instabilities. The concept PBWD is applied considering the performance objective involving those associated with occupant comfort and structural or non-structural damages.

1. Introduction

Tall buildings exhibit complex structural responses under dynamic loads such as the actions of wind. In addition to the dependence on complex and dynamic nature of wind actions, the wind-induced actions on the building are influenced by numerous characteristics of the buildings itself such as its dynamic characteristics, exterior shape, and height. Difficulty in transferring the complex nature of wind and its interaction with buildings led to the development of mathematical models and analysis techniques defining minimum design requirements to ensure safety of the occupants during specific design events. Progressive research and increased computational efficiency over the past couple of decades have produced more elegant solutions to the analysis and design of buildings, the most important one being performance-based design (PBD). PBD proposes that the structure be designed to meet specific performance objectives set forth by the stakeholders. PBD has become a mainstream approach to assess and reduce the risks in rehabilitation of existing structures and in the seismic design of structures. The significant wind related economic losses incurred every year around the world has prompted the researchers to develop methods to

* Corresponding author.
E-mail address: alipour@iastate.edu (A. Alipour).

https://doi.org/10.1016/j.engstruct.2023.115812
Received 20 July 2022; Received in revised form 21 December 2022; Accepted 12 February 2023
Available online 26 May 2023

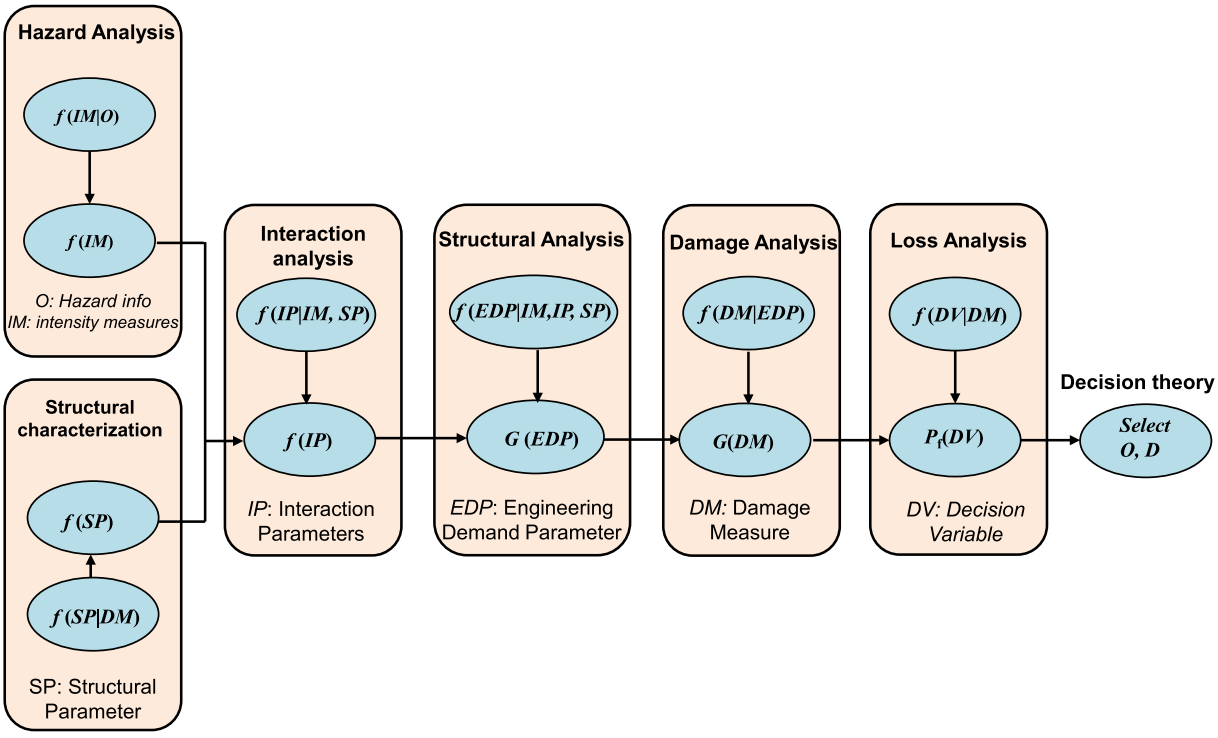

Fig. 1. PBWD methodology flowchart adopted from Petrini (2011).

reframe wind engineering to fully embrace the concepts of PBD.

1.1. Adoption of PBD to performance based wind design

As previously mentioned, PBD has been widely adopted in the seismic design as performance-based seismic design (PBSD) which computes the seismic performance as a multi-level integral based on total probability theorem. Performance-based wind design (PBWD) is majorly drawn from this counterpart in the earthquake engineering community. Ciampoli et. al [1] first converted the Pacific Earthquake Engineering Research Center (PEER) equation to fit into PBWD formulations, which was then followed by others ([2–14]). The advancements made by these researchers have led to development of a working framework for PBWD and an acceptance from the design community to accommodate a PBD philosophy for design of tall buildings under wind. This has resulted in the release of the Pre-standard for Performance Based Wind Design (2019) [15], which is purposed to act complementary to ASCE-07 (2016) [16] and provides guidelines to implement PBWD in building designs to achieve an equal or superior performance objective compared to the prescriptive design methodology provided by [16]. Extensive research has gone into the development of PBWD, and the authors have provided a detailed literature review of such research over the years in Hareendran et. al[17]

The PEER equation was adopted to develop the PBWD framework with modifications to convert the seismic actions to wind actions and is given by equation (1). Fig. 1 shows the flowchart of PBWD as given by [7].

$$P_f(dv) = \int\int\int\int G(DV|DM).|dG(DM|EDP)|.|dG(EDP|IP,IM,SP)|.$$

$$|dG(IP|IM,SP)|.p(IM).p(SP).dDM.dEDP.dIP.dIM.dSP \quad (1)$$

where, *DV* indicates the decision variable that represents specific performance levels such as no collapse, occupant safety, admissible displacements and accelerations of the building, *DM* represents the damage measure indicating the state of damage of different structural components, *EDP* represents the engineering demand parameter that relates the structural response of the structure to the damage occurrence (accelerations and displacements) and *IM* is the intensity measure of the wind event and $G(A|B)$ is the complementary cumulative distribution function (CCDF) of A conditional on B. The parameter, *IP* denotes the interaction parameter representing the wind-structure interaction in the form of aerodynamic loading functions. These interaction parameters, *IP* is strongly dependent on *IM* and structural properties. Despite the extensive advancements that has been made by prior works in formulation of PBWD [17], there are some obstacles in completely adopting a true PBD into PBWD.

(1) Lack of modeling and recognition of post-elastic response of buildings in prior works which will open the potential for unknown behavior after inelastic response at the least and could pose serious threats to the occupants at the most with failure modes that have not been accounted for during the design procedure. In the past few years, the focus on post-elastic behavior has gained attention and is being explored. Some of the notable studies that have studied inelastic response in tall buildings in the context of PBWD are [18–29]. This study aims to bring further focus on the subject and aid this field of research.
(2) Accurately characterizing the interaction between the wind and the building. The self-excited loads that develop because of the interaction of the structural motions and wind loads have not been considered largely in the studies associated with tall buildings, particularly where multi-modes of vibration and non-linearities are involved. The aeroelastic interaction of tall buildings with wind can rarely result in aerodynamic instability but certainly lead to alteration of response due to modification of structural damping and stiffness along all degrees of freedom. The negative aerodynamic damping or modified stiffness due to participation of multiple modes of vibration could be a major concern in flexible structures such as tall buildings.
(3) The importance of occupant comfort which is not accounted for in the PBSD but has major implications when designing the tall

buildings under wind loads. This performance objective has not been widely explored excluding studies such as [30–35]. However, there has been several studies exploring mitigation of structural vibrations to improve overall building performance to attain better occupant comfort levels such as [36–39].

1.2. Objectives of the study

With the computational advancements available today, this paper implements the proposed PBWD methodology by following the true nature of the PBD philosophy considering the nonlinearity in response of buildings and associated uncertainties in the wind loading including effects of self-excited or motion-induced aerodynamic loads. This study aims to address these shortcomings in current adoption of PBD to wind actions and the interaction of structure with the environment using a mathematical formulation that could be used to generate both buffeting and self-excited wind loads for a highly detailed wind load model while emphasizing on occupant comfort as a major additional performance objective to be considered in PBWD. The available approaches in implementing PBWD are limited in capturing the building-wind interaction as they 1) use just synthetic wind loads capturing only the buffeting aspects, and 2) use the results from aerodynamic models of buildings from experiments. As such there is a need for a methodology to capture the true nature of the wind-building interaction as it relates to the impact that the building deformation or speed will have on the change of wind loads on the structure. The limited number of aeroelastic wind tunnel tests – although none used in the PBWD context- do not capture the potential nonlinearities in the building response in higher than design wind speeds that could translate potentially higher wind effects on the building. This study aims to address these major gaps, by providing an analytical model of the wind loads based on both quasi-steady theory (QST) and wind tunnel tests that are conducted on a section model. The load model combined with a strong nonlinear structural modeling platform will provide a means tocapture the full regime of building-wind response. The fact that the methodology requires only results from wind tunnel tests on the section model of the building, makes it robust and achievable to assess buildings of different cross-sections and even buildings that have different cross-sectional shape changes across their height. This methodology to predict the response of an aeroelastic model of a tall building in a boundary-layer wind flow using results from the section-model tests has been successfully used and validated in the past ([34,40]). However, the current methodology extends its application to a full-scale building in the nonlinear regime.

The consideration of the response of tall buildings under the combined action of buffeting and self-excited loads in the time domain would pave the way to consider this important factor in the tall buildings with the possibility to communicate losses in a language that is understandable to stakeholders. This study involves the identification of all 18 flutter derivatives that appear in the three degree-of-freedom (3DOF) self-excited wind loads formulation for two tall buildings with a rectangular plan of aspect ratio 1.5:1. The flutter derivatives are obtained through wind tunnel tests and Quasi-Steady (QS) formulation. The wind tunnel tests are conducted in the Wind Simulation and Testing (WiST) Laboratory at Iowa State University. The methodology to extract the flutter derivatives using wind tunnel tests and quasi-steady formulation is given in future sections of the manuscript. These flutter derivatives are then converted in the time domain using the rational function approximation (RFA) formulation. As mentioned previously, the structural analyses are performed to check for flutter-like divergence in the nonlinear post-elastic response regime of the structures.

Limiting the motion of tall buildings to provide acceptable occupant comfort can be challenging even in moderate wind conditions. Examples of some work accomplished to address this issue have been reviewed by the research team [37,39,35,36,38]. Property developers and building owners continue to face a significant challenge in ensuring occupant comfort in these high-rise structures with complex geometry. But when such motion is not accounted for, the occupants of tall buildings can feel uncomfortable, leading to various psychological and physiological impacts on them and reduced productivity levels in work environments. High building accelerations can cause discomfort to occupants leading to anxiety, headaches, dizziness, and nausea. Hence, setting up acceptable levels of accelerations to ensure sufficient occupant comfort is essential.

Following the highlighted needs to develop a fully developed PBWD framework, the manuscript follows this road map: First, the procedure to characterize the self-excited wind loads in time-domain is provided. Then the nonlinear model of the two case study buildings with two different heights is developed so that a time-domain time-history analysis can be conducted. In the next section, a holistic review of the occupant comfort criteria within the building design community and wind engineering community is provided and the associated thresholds are highlighted within the PBWD framework to assess the performance objectives of the case study buildings. Finally, a detailed review of the effects of consideration of self-excited aerodynamic loads parameters and the proposed steps for the community to adopt PBWD is outlined.

2. Characterizing the interaction of building and wind field

The aerodynamic loads acting on a building consist of the turbulent loads due to fluctuating winds known as buffeting loads and the aeroelastic loads resulting from the interaction of the structural motions with wind referred as self-excited loads. Flutter instability can be a significant concern in flexible structures such as long-span bridges and tall

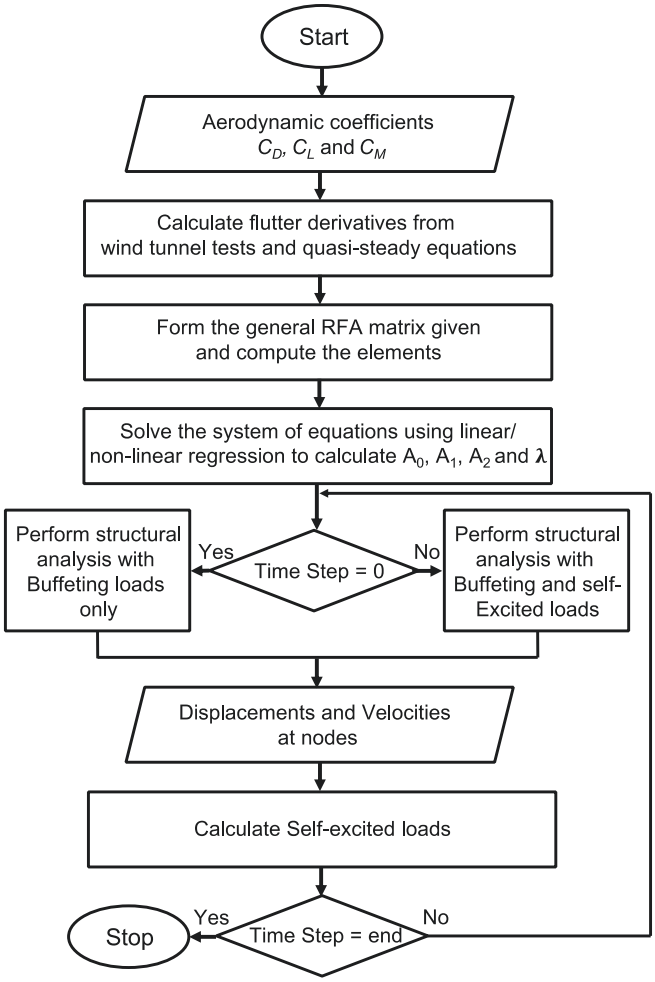

Fig. 2. Structural analysis model with iterative addition of self-excited forces.

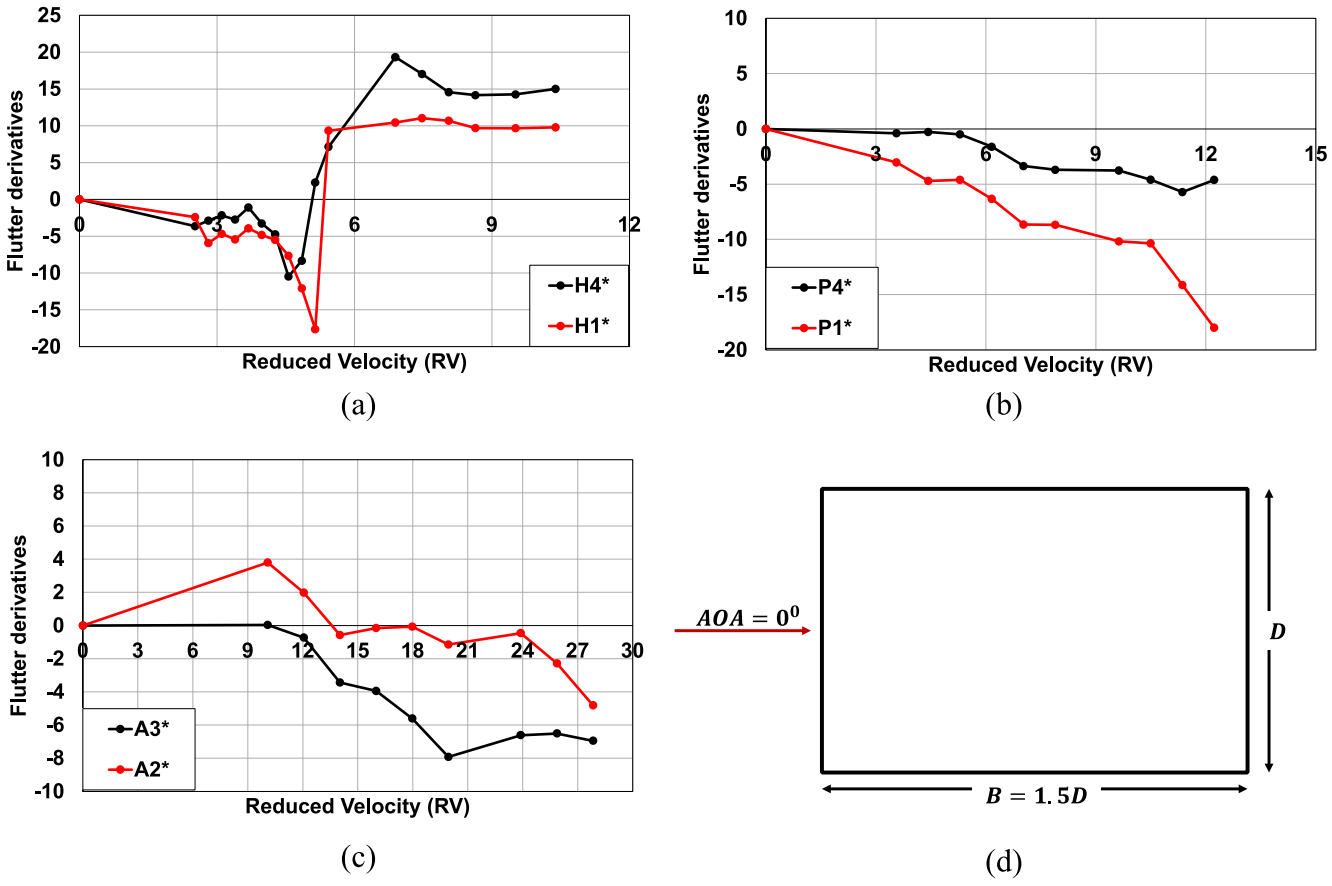

Fig. 3. Flutter derivatives obtained from wind tunnel tests for a rectangular section model with aspect ratio of 1.5:1 (a) H1* and H4* (b) P1* and P4* (c) A2* and A3* and (d) cross section of the model showing the angle of attack at 0o.

buildings. Although flutter instability that is caused by self-excited loads generally doesn't occur in tall buildings within their design wind speeds but certainly needs to be considered in a wind-structure interaction analysis, particularly when buildings become increasingly slender and may enter post-elastic range of response with the implementation of ASCE Prestandard [15]. The wind-induced vibrations in a structure gets amplified with diverging motion at or beyond a critical wind speed known as flutter speed leading to instability. Over the past several decades, beginning in the 1970s, numerous studies have been conducted to accurately describe the flutter phenomenon of flexible structures. But nearly all of these studies have been focused on the self-excited response of bridges ([3–4,41–43]). Chowdhury and Sarkar ([44–46]) extracted all eighteen flutter derivatives from 3DOF experimental studies. The flutter derivatives are used to express self-excited loads and estimate the occurrence of flutter phenomenon in the frequency domain whereas the rational function coefficients (RFCs) or rational functions or indicial functions are used in the time domain. Chowdhury [46] developed methods to extract rational functions directly from wind tunnel section model studies using free vibrations. Sarkar et. al [34,43,46] extended the studies to extract RFCs using a force-vibration technique and calculate the dynamic wind loads acting on structures in the time domain. Chen et. al [42] also developed rational function approximation formulation based on flutter derivatives using an optimization technique and validated the formulation in 2DOF for bridge sections. Mishra [47] used an optimization technique to obtain RFCs using all eighteen flutter derivatives in 3DOF.

Table 1
Aerodynamic Coefficients for rectangular section with $B/D = 1.5$.

AOA	C_D	C_L	C_M	$dC_D/d\theta$	$dC_L/d\theta$	$dC_M/d\theta$
0	1.21	0	0	0.00	−3.55	−0.573
34	1.26	0.38	0.057	−3.00	−0.23	0.203
90	2.93	0	0	0.00	−2.74	−0.394

Note: AOA (Angle of Attack): wind direction at 0 degree AOA is along the longer dimension B and it is positive in counterclockwise direction.

The flutter derivatives can be obtained experimentally from wind tunnel tests or approximately obtained by using mathematical formulations such as QST based on static aerodynamic load coefficients (lift, drag, moment) and their derivatives. For flexible buildings such as tall buildings, apart from identifying the flutter speed (if any), the time-dependent variation of self-excited loads and its influence on the structural damping/stiffness and resulting motion at wind speeds below the flutter speed needs to be explored. The self-excited load calculation presented here follows the RFA formulation presented by Chowdhury and Sarkar [44–46].

2.1. Numerical formulations of aerodynamic actions on tall buildings

A tall building under the action of incident wind speeds can have 3DOF response, namely *h*, *p* and α, corresponding to the displacements in lateral, vertical, and torsional directions. The equation of motion corresponding to each DOF is given below:

$$m_h\ddot{h} + c_h\dot{h} + k_h h = L_{se} \tag{2}$$

$$m_p\ddot{p} + c_p\dot{p} + k_p p = D_{se} \tag{3}$$

$$I_\alpha\ddot{\alpha} + c_\alpha\dot{\alpha} + k_\alpha\alpha = M_{se} \tag{4}$$

where m_h, m_p are the mass per unit length, I_α is the mass moment of inertia about the center of mass of the cross section, c_h, c_p and c_α are the

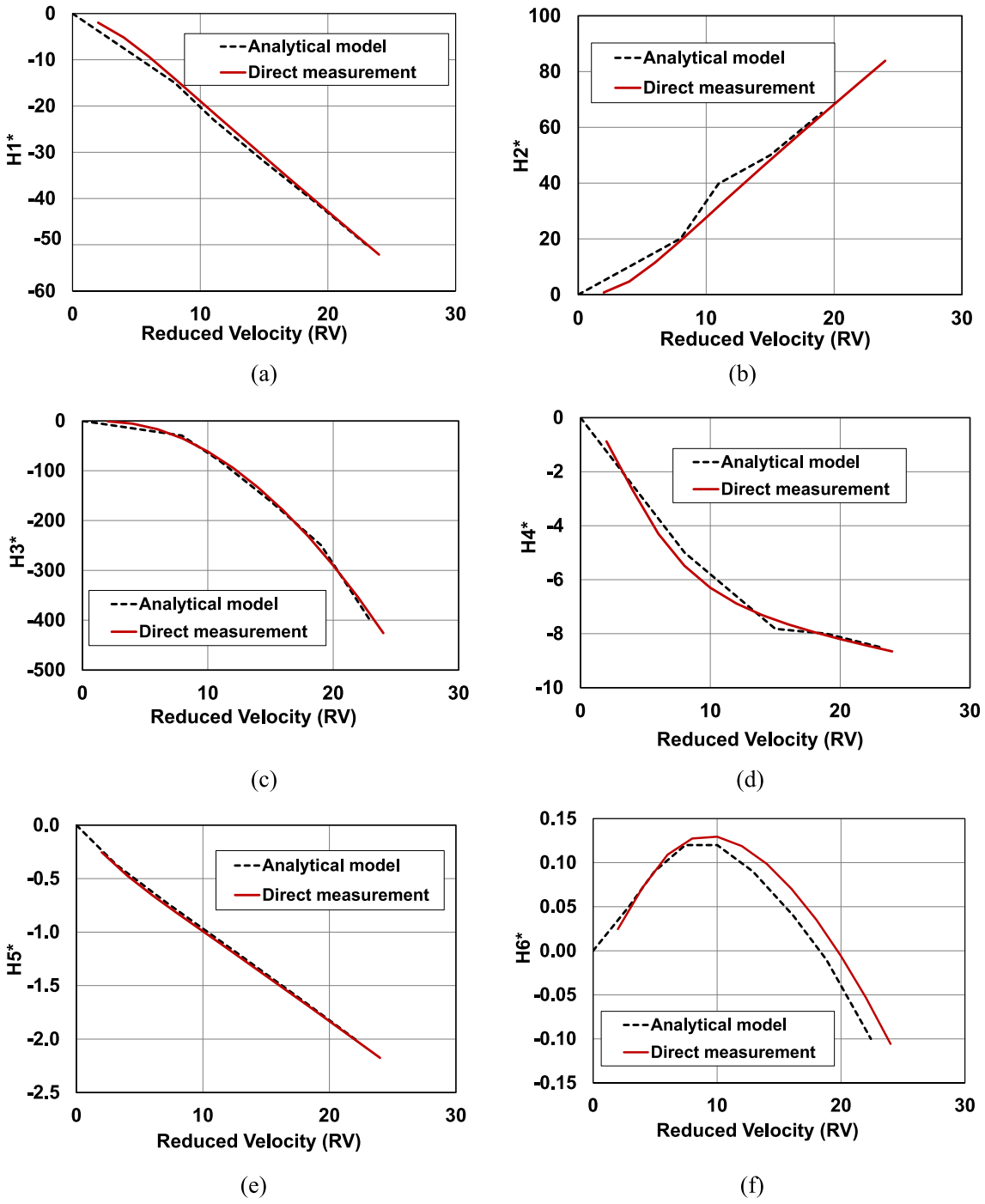

Fig. 4. Comparison of flutter derivatives obtained by numerically calculating from measured RFC functions (Analytical model) and from direct measurement (Sarkar & Sauder (2017)) corresponding to vertical motion in 3 DOF system for a rectangular section model with an aspect ratio of 5:1 (a) H1* (b) H2* (c) H3* (d) H4* (e) H5* and (f) H6*.

damping coefficients, k_h, k_p and k_α are the stiffness coefficients of the dynamic system. The derivatives $\left(\dot{h},\right), \left(\ddot{h}\right)$ of h, p and α with time are the velocity and acceleration responses of the structure.

Self-excited loads (lift L_{se}, drag D_{se}, and moment M_{se}) per unit length in the vertical, lateral, and torsional directions in Eqns. 2–4 can be written in terms of flutter derivatives. These expressions developed by Scanlan [48] for 2DOF and later extended for 3DOF are given as follows:

$$L_{se} = \frac{1}{2}\rho U^2 B\left[KH_1^*\frac{\dot{h}}{U} + KH_2^*\frac{B\dot{\alpha}}{U} + K^2H_3^*\alpha + K^2H_4^*\frac{h}{B} + KH_5^*\frac{\dot{p}}{U} + K^2H_6^*\frac{p}{B}\right] \quad (5)$$

$$D_{se} = \frac{1}{2}\rho U^2 B\left[KP_1^*\frac{\dot{p}}{U} + KP_2^*\frac{B\dot{\alpha}}{U} + K^2P_3^*\alpha + K^2P_4^*\frac{p}{B} + KP_5^*\frac{\dot{h}}{U} + K^2P_6^*\frac{h}{B}\right] \quad (6)$$

$$M_{se} = \frac{1}{2}\rho U^2 B^2\left[KA_1^*\frac{\dot{h}}{U} + KA_2^*\frac{B\dot{\alpha}}{U} + K^2A_3^*\alpha + K^2A_4^*\frac{h}{B} + KA_5^*\frac{\dot{p}}{U} + K^2A_6^*\frac{p}{B}\right] \quad (7)$$

where ρ is the density of air, U is the mean crosswind velocity, B is the width of the building, K is the non-dimensional frequency given by $K = \frac{B\omega}{U}$. H_1^* to H_6^*, P_1^* to P_6^*, and A_1^* to A_6^* are the flutter derivatives. Substituting equations (5) to (7) into the right-hand side of equations (2)

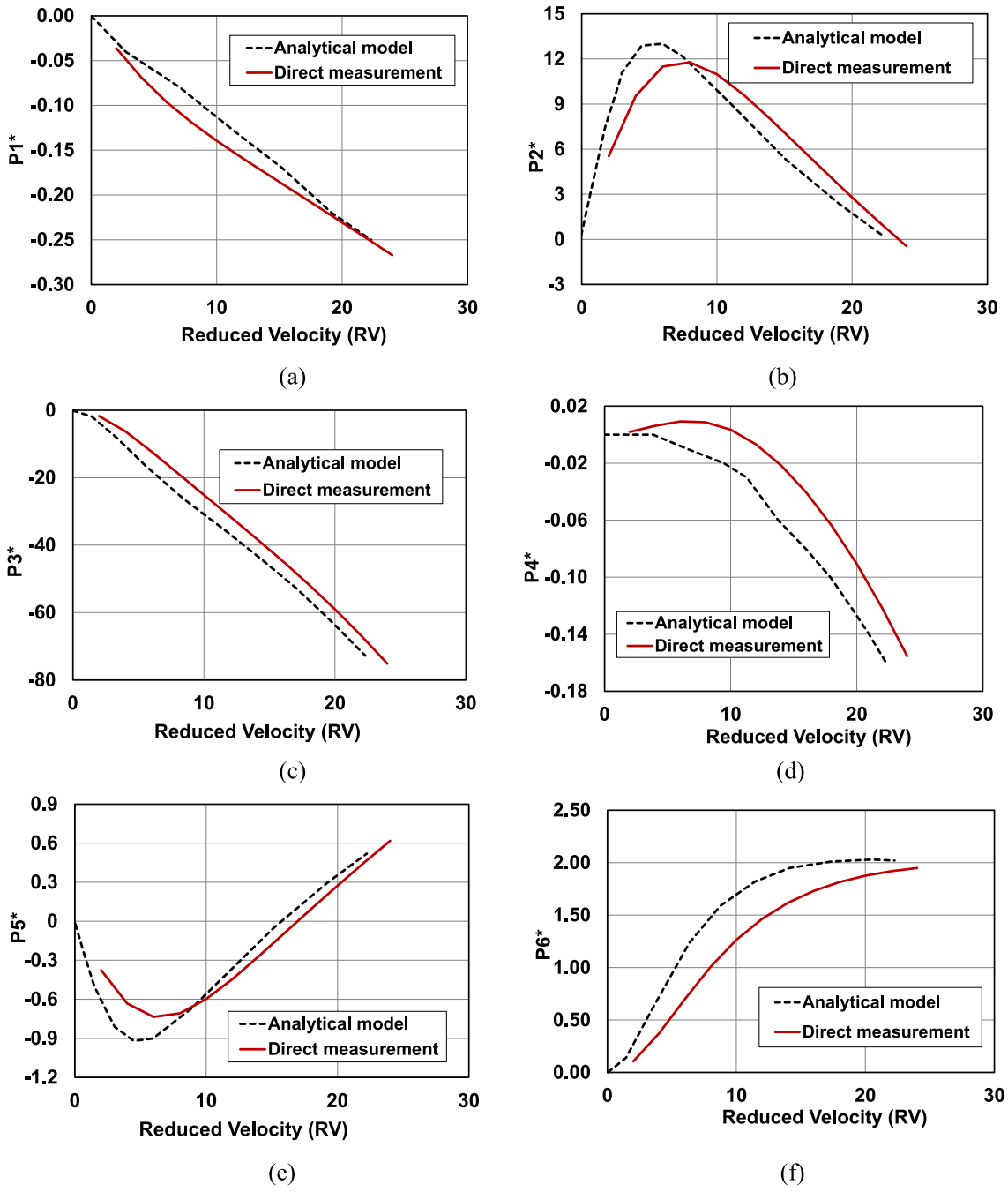

Fig. 5. Comparison of flutter derivatives obtained by numerically calculating from measured RFC functions (Analytical model) and from direct measurement (Sarkar & Sauder(2017)) corresponding to lateral motion in 3 DOF system for a rectangular section model with an aspect ratio of 5:1 (a) P1* (b) P2* (c) P3* (d) P4* (e) P5* and (f) P6*.

to (4) and writing them in matrix form gives the equation of motion as:

$$\boldsymbol{M}\ddot{\boldsymbol{q}} + \boldsymbol{C}\dot{\boldsymbol{q}} + \boldsymbol{K}\boldsymbol{q} = \frac{B}{U}\boldsymbol{V}_f\boldsymbol{Q}_0\dot{\boldsymbol{q}} + \boldsymbol{V}_f\boldsymbol{Q}_1 \tag{8}$$

where $\boldsymbol{q}$ is the non-dimensional displacement vector given by $\boldsymbol{q} = [h/B \;\; p/B \;\; \alpha]$. Coefficient matrices in equation (8) are given by:

$$\boldsymbol{M} = \begin{bmatrix} mB & 0 & 0 \\ 0 & mB & 0 \\ 0 & 0 & I_\alpha \end{bmatrix} \tag{9}$$

$$\boldsymbol{C} = \begin{bmatrix} 2\zeta_h\omega_h mB & 0 & 0 \\ 0 & 2\zeta_p\omega_p mB & 0 \\ 0 & 0 & 2\zeta_\alpha\omega_\alpha I_\alpha \end{bmatrix} \tag{10}$$

$$\boldsymbol{K} = \begin{bmatrix} {\omega_h}^2 mB & 0 & 0 \\ 0 & {\omega_p}^2 mB & 0 \\ 0 & 0 & {\omega_\alpha}^2 I_\alpha \end{bmatrix} \tag{11}$$

$$\boldsymbol{V}_f = \begin{bmatrix} 0.5\rho U^2 B & 0 & 0 \\ 0 & 0.5\rho U^2 B & 0 \\ 0 & 0 & 0.5\rho U^2 B^2 \end{bmatrix} \tag{12}$$

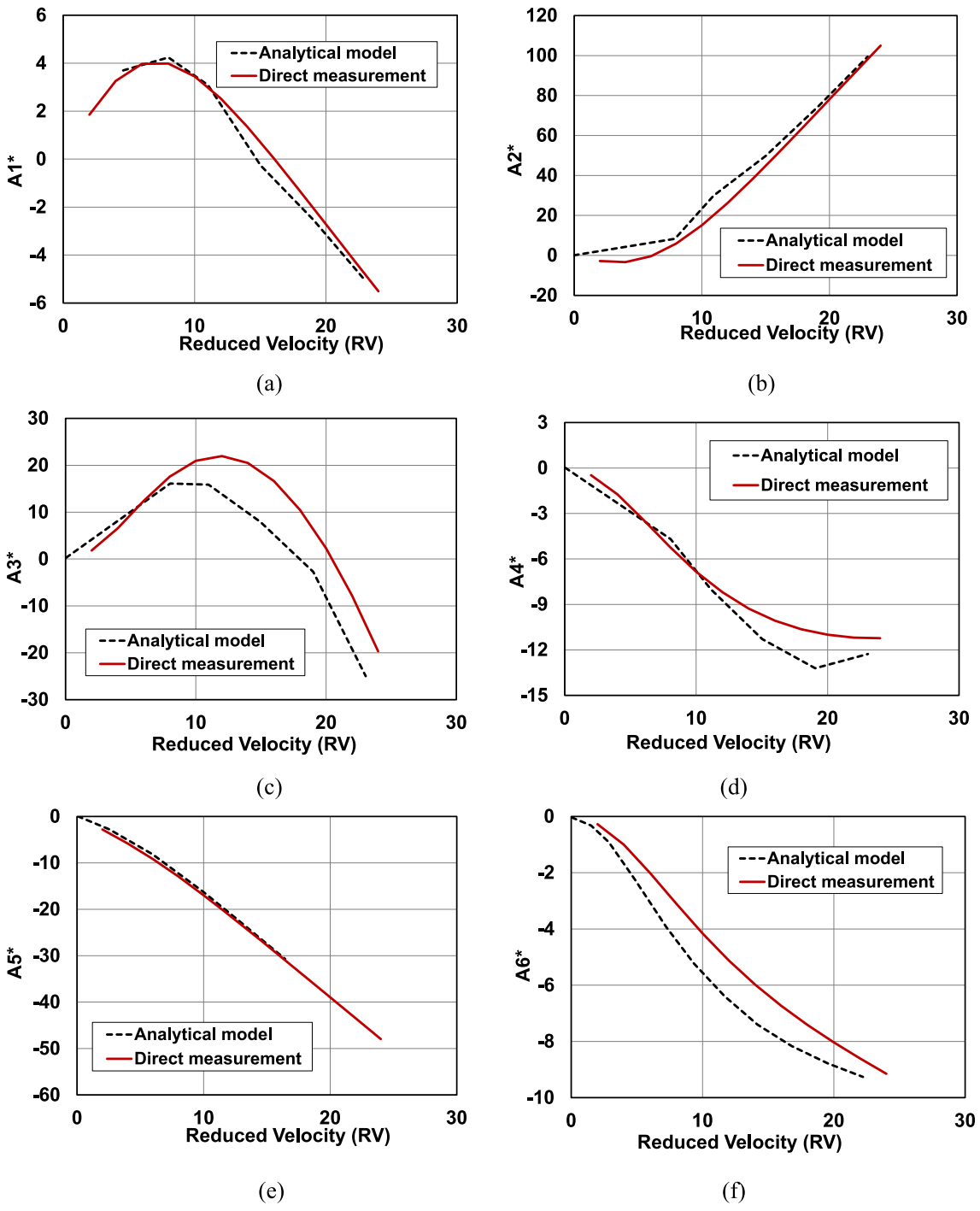

Fig. 6. Comparison of flutter derivatives obtained by numerically calculating from measured RFC functions (Analytical model) and from direct measurement (Sarkar & Sauder) corresponding to torsional motion in 3 DOF system for a rectangular section model with an aspect ratio of 5:1 (a) A1* (b) A2* (c) A3* (d) A4* (e) A5* and (f) A6*.

$$\boldsymbol{Q}_0 = \begin{bmatrix} KH_1^* & KH_5^* & KH_2^* \\ KP_5^* & KP_1^* & KP_2^* \\ KA_1^* & KA_5^* & KA_2^* \end{bmatrix} \tag{13}$$

$$\boldsymbol{Q}_1 = \begin{bmatrix} K^2H_4^* & K^2H_6^* & K^2H_3^* \\ K^2P_6^* & K^2P_4^* & K^2P_3^* \\ K^2A_4^* & K^2A_6^* & K^2H_3^* \end{bmatrix} \tag{14}$$

The right-hand side of equation (8) can be combined into a single matrix and written in the complex form of $\boldsymbol{Q}$ in frequency domain (K) by combining $\boldsymbol{Q_1}$ and $\boldsymbol{Q_o}$ and $\boldsymbol{q}$ is in time domain (t):

$$\boldsymbol{M\ddot{q} + C\dot{q} + Kq = V_f Qq} \tag{15}$$

where rational function matrix $\boldsymbol{Q}$ is given by:

$$\boldsymbol{Q} = \begin{bmatrix} K^2(H_4^* + iH_1^*) & K^2(H_6^* + iH_5^*) & K^2(H_3^* + iH_2^*) \\ K^2(P_6^* + iP_5^*) & K^2(P_4^* + iP_1^*) & K^2(P_3^* + iP_2^*) \\ K^2(A_4^* + iA_1^*) & K^2(A_6^* + iA_5^*) & K^2(H_3^* + iA_2^*) \end{bmatrix} \tag{16}$$

Taking the Laplace transform of equation (15) under the assumption of zero initial conditions gives the equations of motion for the 3DOF system as:

$$(\boldsymbol{M}s^2 + \boldsymbol{C}s + \boldsymbol{K})L(q) = \boldsymbol{V}_f \widehat{\boldsymbol{Q}} L(q) \tag{17}$$

where L in the above equation denotes the Laplace operator.

The approximation of rational function matrix $\boldsymbol{Q}$ in frequency domain (K) as in Eqn. (16) or $\widehat{\boldsymbol{Q}}$ in Laplace domain ($p = iK$) in Eqn. (17), where $\boldsymbol{Q}_{ij}$ or $\widehat{\boldsymbol{Q}}_{ij}$ are complex rational functions in terms of flutter derivatives (Eqn. (16)), can be expressed by RFC's that allows the conversion of the self-excited loads into linear time-invariant state-space realizations. The elements of the rational function matrix $\widehat{\boldsymbol{Q}}$ can be expressed as:

$$\widehat{\boldsymbol{Q}_{ij}}(p) = (\boldsymbol{A}_0)_{ij} + (\boldsymbol{A}_1)_{ij}p + (\boldsymbol{A}_2)_{ij}p^2 + \sum_{l=1}^{n_l} (\boldsymbol{A}_{l+2})_{ij}\frac{1}{p+\lambda_l} \tag{18}$$

where $\widehat{\boldsymbol{Q}}$ represents the rational function matrix and the above equation is the Rational Function Approximation (RFA) of $\widehat{\boldsymbol{Q}}$ in the non-dimensional Laplace variable, p, that is given as $p = \frac{sB}{U} = iK$ where s is the non-dimensional time given as $s = \frac{Ut}{B}$. The fractions $(\boldsymbol{A}_{l+2})_{ij}\frac{1}{p+\lambda_l}$ are the lag terms and $\boldsymbol{A_0}$, $\boldsymbol{A_1}$, $\boldsymbol{A_2}$ along with $A_{l+2,\ l=1\text{-}n1}$ are RFCs. The number of partial fractions is denoted by n_l and it depends on the compromise in precision that can be made in the calculations. The value of n_l generally varies between 2 and 4. Chen and Matsumoto [41] have taken $n_l = 2$ or 2 lag terms in their analyses and Mishra [47] has used $n_l = 4$ or 4 lag terms in the analyses. However, the studies by Sarkar [44] have shown that the use of 1 to 2 lag terms provides near accurate results. Hence, to simplify the calculations by reducing the number of unknowns, only one lag term is considered in this study. In the least-squares approximation of RFA, the same denominator of $\frac{1}{p+\lambda_l}$ is used in every element of the matrix $\widehat{\boldsymbol{Q}}$ to reduce the number of additional aerodynamic states resulting in the state space. $\boldsymbol{A_0}$, $\boldsymbol{A_1}$, $\boldsymbol{A_2}$ and $\boldsymbol{A_{l+2}}$ are 3×3 matrices for a 3DOF system containing coefficients of the rational functions or RFC's. $\boldsymbol{A_0}$ and $\boldsymbol{A_1}$ are the aerodynamic stiffness and damping matrices, respectively. $\boldsymbol{A_2}$ is the additional aerodynamic mass due to wind loads and is generally negligible. Hence equation (19) can be rewritten by neglecting $\boldsymbol{A_2}$ and retaining 1-lag term as:

$$\widehat{\boldsymbol{Q}}(p) = \boldsymbol{A}_0 + \boldsymbol{A}_1 p + \boldsymbol{A}_2 \frac{1}{p+\lambda_1} \tag{19}$$

The approximation of $\boldsymbol{A_n}$ ($n = 0$ to 2) can be done by linear or nonlinear optimization of least squares. The transformation of rational function formulation from the Laplace domain to time domain is given by Cao and Sarkar [43] for 2DOF and further extended to 3DOF by Sauder and Sarkar [49]. The self-excited load formulations for 3DOF system in time domain in terms of RFCs are given below:

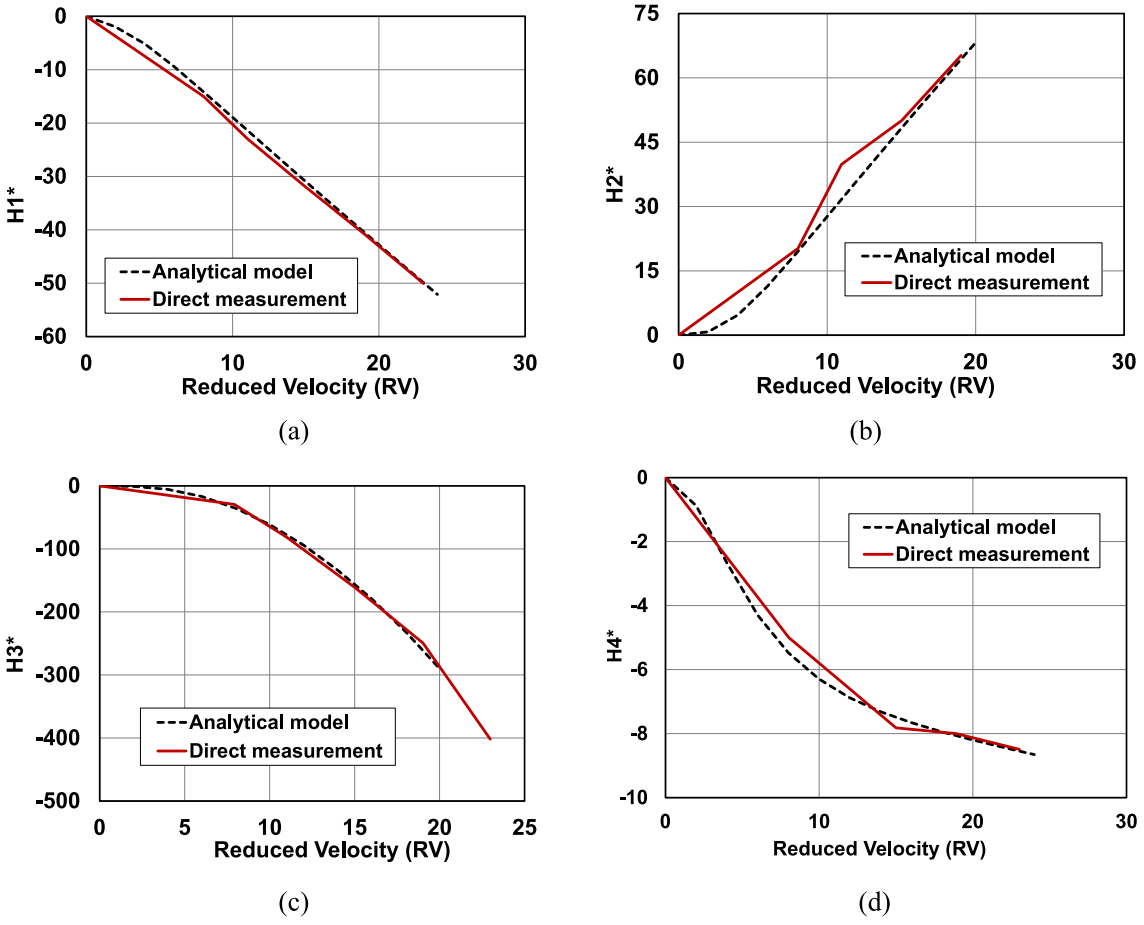

Fig. 7. Comparison of flutter derivatives obtained by numerically calculating from measured RFC functions (Analytical model) and from direct measurement (Sarkar & Sauder) corresponding to vertical motion in 2 DOF system for a rectangular section model with an aspect ratio of 5:1 (a) H1* (b) H2* (c) H3* and (d) H4*.

$$L_{se}(t) = \frac{1}{2}\rho U^2 B\Big\{ [(A_0)_{11} + (A_2)_{11}]\frac{h}{B} + (A_1)_{11}\frac{\dot{h}}{U} - (A_2)_{11}\frac{\lambda_L U}{B^2}\int_0^t e^{-\frac{U}{B}\lambda_l(t-\tau)}h(\tau)d\tau + [(A_0)_{12} + (A_2)_{12}]p + (A_1)_{12}\frac{\dot{p}}{U}B - (A_2)_{12}\frac{\lambda_L U}{B}\int_0^t e^{-\frac{U}{B}\lambda_l(t-\tau)}p(\tau)d\tau + [(A_0)_{13} + (A_2)_{13}]\alpha + (A_1)_{13}\frac{B}{U}\dot{\alpha} - (A_2)_{13}\frac{\lambda_L U}{B}\int_0^t e^{-\frac{U}{B}\lambda_l(t-\tau)}\alpha(\tau)d\tau \Big\} \quad (20)$$

$$D_{se}(t) = \frac{1}{2}\rho U^2 B\Big\{ [(A_0)_{21} + (A_2)_{21}]\frac{h}{B} + (A_1)_{21}\frac{\dot{h}}{U} - (A_2)_{21}\frac{\lambda_D U}{B^2}\int_0^t e^{-\frac{U}{B}\lambda_D(t-\tau)}h(\tau)d\tau + [(A_0)_{22} + (A_2)_{22}]p + (A_1)_{22}\frac{\dot{p}}{U}B - (A_2)_{22}\frac{\lambda_D U}{B^2}\int_0^t e^{-\frac{U}{B}\lambda_D(t-\tau)}p(\tau)d\tau + [(A_0)_{23} + (A_2)_{23}]\alpha + (A_1)_{23}\frac{B}{U}\dot{\alpha} - (A_2)_{23}\frac{\lambda_D U}{B}\int_0^t e^{-\frac{U}{B}\lambda_D(t-\tau)}\alpha(\tau)d\tau \Big\} \quad (21)$$

$$M_{se}(t) = \frac{1}{2}\rho U^2 B^2\Big\{ [(A_0)_{31} + (A_2)_{31}]\frac{h}{B} + (A_1)_{31}\frac{\dot{h}}{U} - (A_2)_{31}\frac{\lambda_M U}{B^2}\int_0^t e^{-\frac{U}{B}\lambda_M(t-\tau)}h(\tau)d\tau + [(A_0)_{32} + (A_2)_{32}]p + (A_1)_{32}\frac{\dot{p}}{U}B - (A_2)_{32}\frac{\lambda_M U}{B^2}\int_0^t e^{-\frac{U}{B}\lambda_M(t-\tau)}p(\tau)d\tau + [(A_0)_{33} + (A_2)_{33}]\alpha + (A_1)_{33}\frac{B}{U}\dot{\alpha} - (A_2)_{33}\frac{\lambda_M U}{B}\int_0^t e^{-\frac{U}{B}\lambda_M(t-\tau)}\alpha(\tau)d\tau \Big\} \quad (22)$$

2.2. Aeroelastic coefficients in the model

As mentioned earlier, the flutter derivatives can be obtained from experimental testing or using the static aerodynamic load coefficients and their derivatives in QST formulation. The 6 direct flutter derivatives (H_1*, H_4*, P_1*, P_4*, A_2*, and A_3*) out of the 18 flutter derivatives (Eqns. 5–7) in a 3DOF system for a rectangular cross section with an aspect ratio (width B to depth D) of 1.5:1 used in this study were obtained experimentally by Hou and Sarkar [34]. They extracted flutter derivatives from section model tests with the same aspect ratio as the tall building in this paper. Comparison of structural responses calculated using such coefficients with those obtained from scaled full building wind tunnel tests showed good agreements up to a mean hourly wind speed of 22.9 m/s or a 3 sec gust of 47.9 m/s at 10 m height. The divergence of results for higher wind speeds can be mainly attributed to the rectangular cross section of the building which is sensitive to large

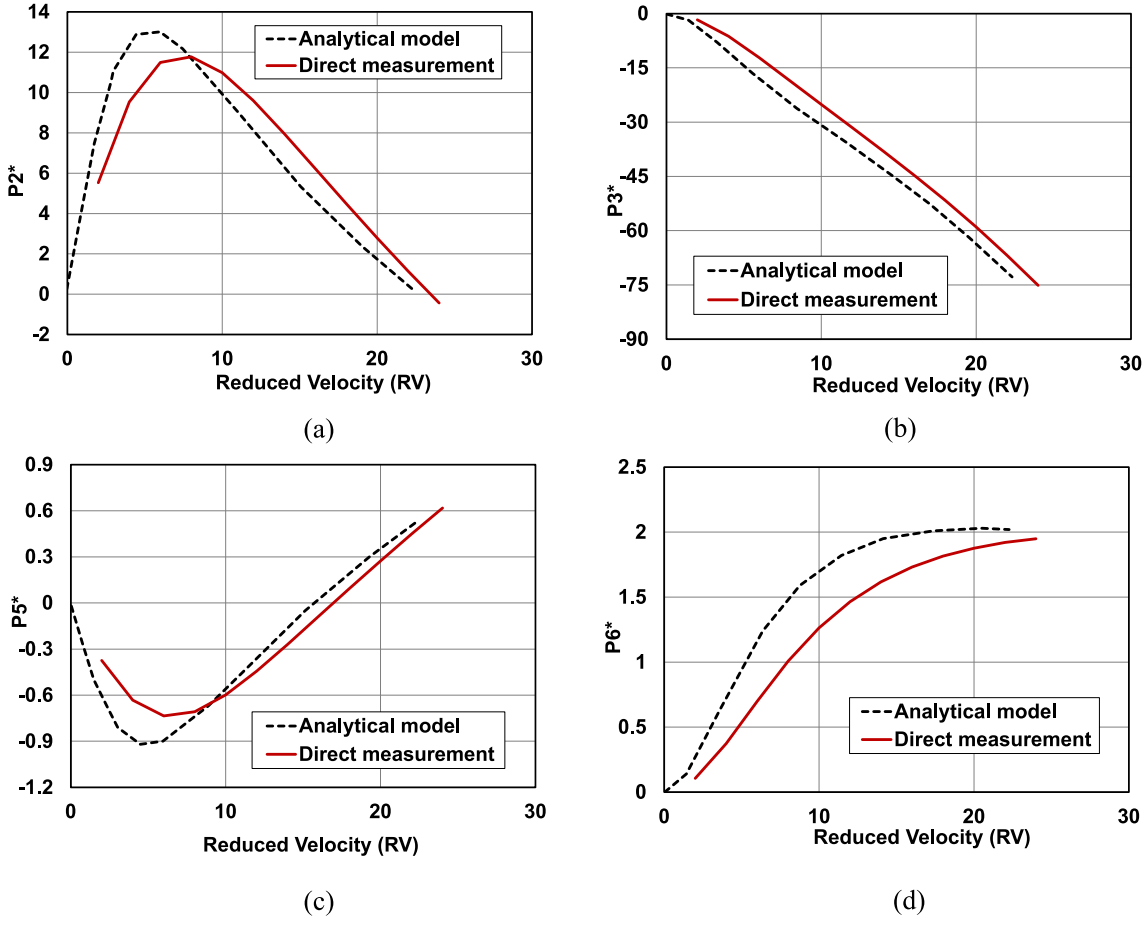

Fig. 8. Comparison of flutter derivatives obtained by numerically calculating from measured RFC functions (Analytical model) and from direct measurement (Sarkar & Sauder) corresponding to lateral motion in 2 DOF system for a rectangular section model with an aspect ratio of 5:1 (a) P2* (b) P3* (c) P5* and (d) P6*.

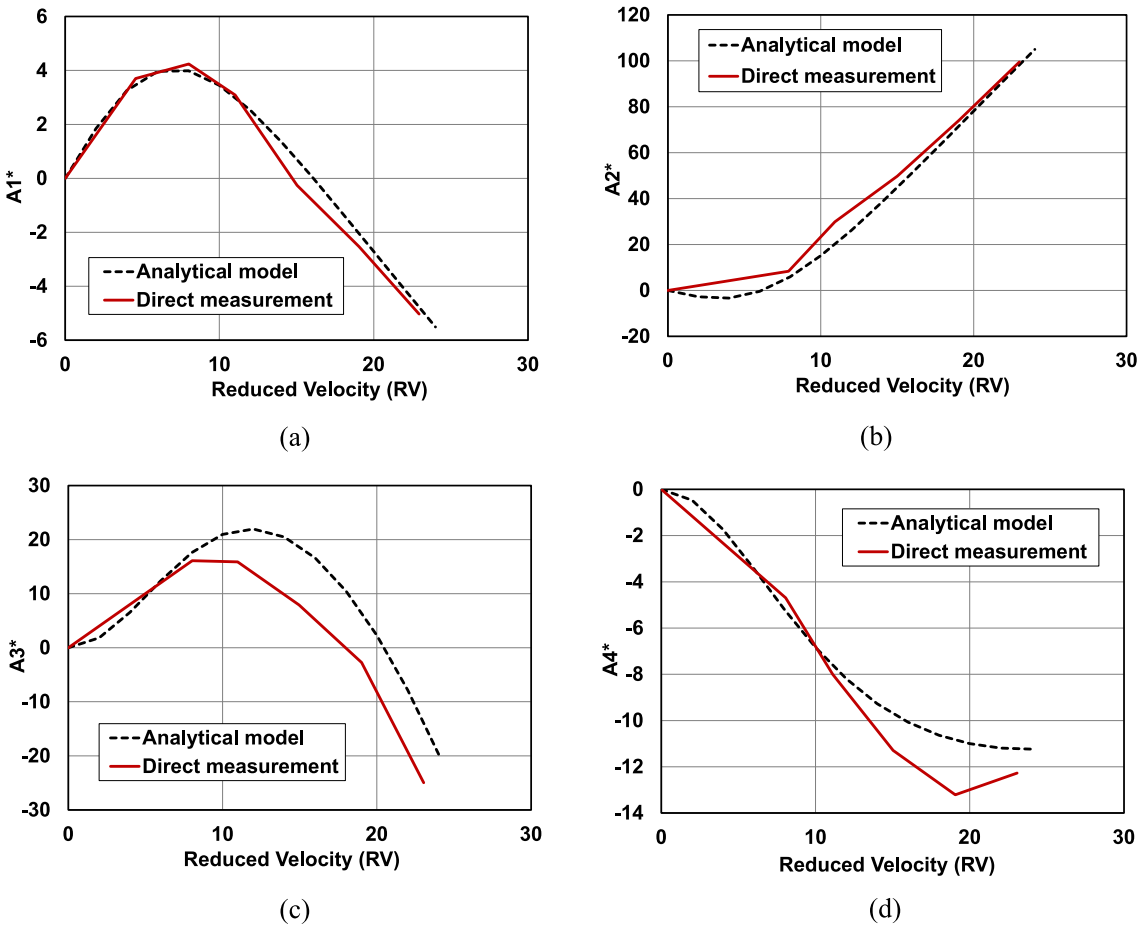

Fig. 9. Comparison of flutter derivatives obtained by numerically calculating from measured RFC functions (Analytical model) and from direct measurement (Sarkar & Sauder) corresponding to torsional motion in 2 DOF system for a rectangular section model with an aspect ratio of 5:1 (a) A1* (b) A2* (c) A3* and (d) A4*.

across wind responses due to aeroelastic effects leading to reduction in damping in across-wind direction and the resulting aeroelastic instability at higher wind speeds. The authors acknowledge this limitation to the adaption of linearized aeroelastic load model based on a section model to full scale 3D model at higher wind speeds used in this study and identify this as a potential improvement that can be explored in future studies. Eight out of the other 12 indirect flutter derivatives, responsible for aerodynamic coupling between the various degrees of freedom, were obtained following the quasi-steady formulation given by Scanlan [48] and [46]. Equations (23) to (30) gives the QST formulae using static aerodynamic load coefficients (C_D, C_L and C_M) that were used here. The QST formulation for the remaining 4 flutter derivatives (H_6*, P_6*, A_4* and A_6*) is not available and hence these are taken to be zero; based on the assumption that the aerodynamics stiffness terms are generally small, and hence negligible.

The advantage of expressing the self-excited loads in time domain using RFCs is that it enables multimode flutter analysis without iterations and without doing modal analysis. The direct extraction of RFCs requires testing the section model of a geometrically-scaled cross section of a structure in the wind tunnel under free or forced vibration, recording the corresponding responses or responses and aerodynamic loads in the time domain, and then extracting the RFCs. The RFCs can be also indirectly obtained because these are related to the flutter derivatives using the least-squares RFA method/Minimum state RFA method as mentioned earlier. Thus, this indirect approach was used here that involves the extraction of flutter derivatives from wind tunnel experiments/QST and then converting to RFA's in the Laplace domain. The procedure outlined above explains the development of RFA's using flutter derivatives in the Laplace domain. Fig. 2 shows the step-by-step process involved in the wind load calculation in time domain and iterative structural analysis to include the effects of self-excited loads.

The flutter derivatives obtained from the 3DOF experimental tests conducted by Hou and Sarkar [34,40] for a rectangular section model (aspect ratio B/D = 1.5) is given in Fig. 3. The figures show the variation of the flutter derivative with respect to the normalized form of wind velocity or reduced velocity, RV, which is a function of the structural frequency given as $RV = U/nB$ where n is the structural frequency n_h, n_p or n_α at zero wind speed corresponding to the flutter derivatives associated with H_i^*, P_i^*, and A_i^*, respectively. The expressions to calculate flutter derivatives using the static aerodynamic load coefficients and their derivatives with angle of attack (θ) are given below:

$$H_2^* = \frac{2}{K}\left(\frac{dC_L}{d\theta}\right) \tag{23}$$

$$H_3^* = -\frac{2}{K^2}\left(\frac{dC_L}{d\theta}\right) \tag{24}$$

$$H_5^* = \frac{2}{K}C_L \tag{25}$$

$$P_2^* = -\frac{1}{4K}\left(\frac{dC_D}{d\theta} - C_L\right) \tag{26}$$

$$P_3^* = \frac{1}{K^2}\left(\frac{dC_D}{d\theta}\right) \tag{27}$$

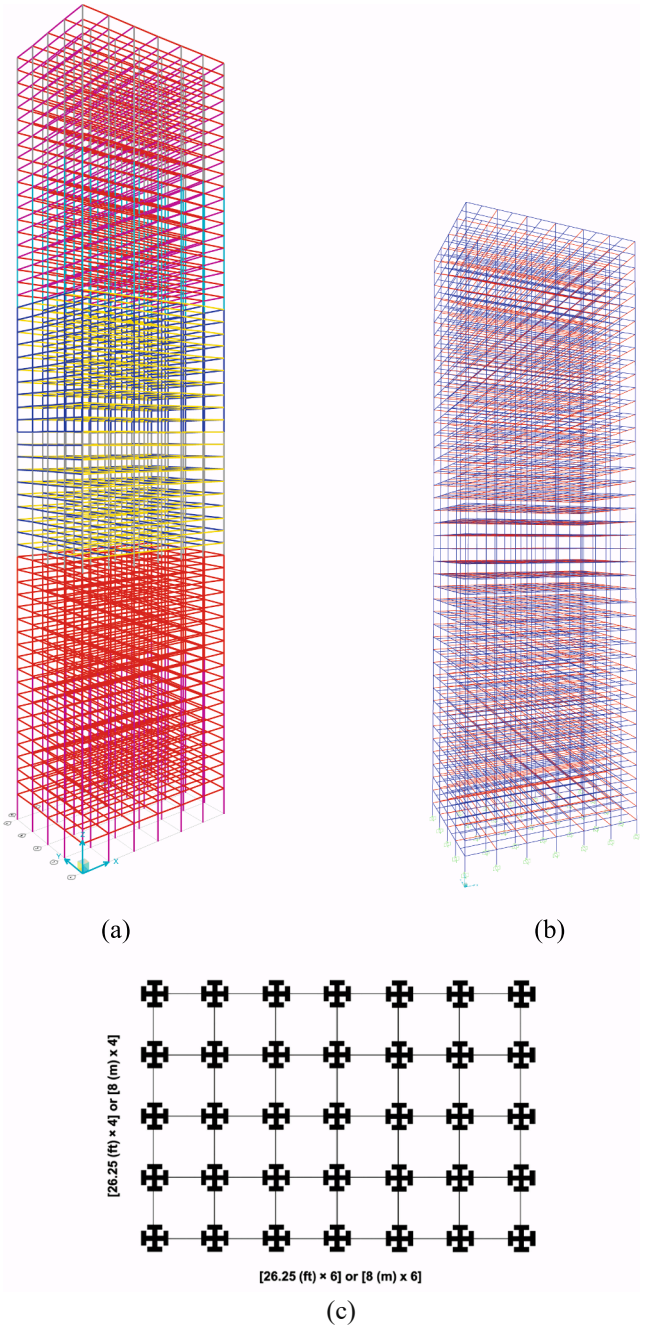

Fig. 10. 3-D representation of the two case-study tall steel frame buildings (a) B-60 and (b) B-44 and (c) plan view of the buildings (Aspect ratio = 1.5:1).

$$P_5^* = \frac{1}{K}\left(\frac{dC_D}{d\theta} - C_L\right) \tag{28}$$

$$A_1^* = \frac{1}{K}\left(\frac{dC_M}{d\theta}\right) \tag{29}$$

$$A_5^* = -\frac{2}{K}C_M \tag{30}$$

where C_D, C_L and C_M are the drag, lift and moment coefficients, $C'_L = dC_L/d\theta$ and $C'_m = dC_M/d\theta$ are the derivatives of the lift and moment coefficients. The values of the coefficients obtained for three different angle of attacks (AOAs) are listed in Table 1.

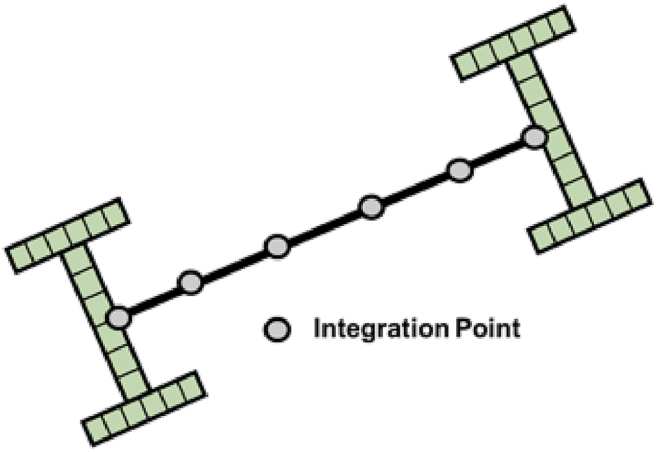

Fig. 11. Force-Based Element showing the integration points and cross-section.

2.3. Validation of algorithm based on past experimental results

The RFCs defined in the self-excited load formulation in time domain with one lag term (Eqns. 20–22), as presented in the previous section, were identified for a rectangular section for both 2DOF and 3DOF by [49] that used a section model with a forced-vibration system. The RFCs for the 2DOF system in this study were validated for a 2DOF system by calculating the 8 flutter derivatives associated with the 2DOF system from the RFCs and comparing them with known values from the literature. The rectangular section chosen in the validations have a width-to-depth (B/D) ratio of 5:1 in both the cases with the length, width and depth of the model being 0.533 m, 0.16 m and 0.032 m, respectively. In the numerical method used in the present study to extract the RFCs of a structural cross-section from its known flutter derivatives, the self-excited loads on the section model in a 2DOF or 3DOF forced vibration system, subject to sinusoidal motions of fixed amplitude, are generated first using the flutter derivatives and the RFCs are then extracted from the self-excited load time histories using an algorithm. The section model was driven with sinusoidal motions at constant amplitudes at 1.06 Hz along each of the two or three DOF systems at three different wind speeds of 5 m/s, 6.5 m/s and 9.4 m/s and the time histories of the self-excited loads were generated using the flutter derivatives in this study. Using the analytical framework presented in this paper, the RFCs that were extracted for the 3DOF case are given below.

$$A_0 = \begin{bmatrix} -17.0477 & 0.3127 & -53.1887 \\ 3.1194 & 0.0011 & -43.3839 \\ -5.8454 & -5.9833 & 29.1643 \end{bmatrix} \tag{a1}$$

$$A_1 = \begin{bmatrix} -1.6112 & -0.8600 & 29.1141 \\ -2.4141 & -0.0936 & 31.7806 \\ 7.2563 & -7.2220 & -15.0747 \end{bmatrix} \tag{a2}$$

$$A_2 = \begin{bmatrix} 23.4979 & -0.4038 & 27.6582 \\ -3.5769 & -0.0286 & 43.4162 \\ 4.5281 & 4.6546 & -29.9559 \end{bmatrix} \tag{a3}$$

$\lambda_L = 1.3573, \lambda_D = 0.1.1155$ and. $\lambda_M = 0.7131$

The RFCs extracted for the 2-DOF case are given below.

$$A_0 = \begin{bmatrix} -12.22 & -6.8525 \\ -6.0545 & 23.6398 \end{bmatrix} \tag{b1}$$

$$A_1 = \begin{bmatrix} -5.8969 & -0.0109 \\ 6.8397 & -11.3148 \end{bmatrix} \tag{b2}$$

$$A_2 = \begin{bmatrix} 14.7625 & -38.611 \\ 3.7852 & -18.8746 \end{bmatrix} \tag{b3}$$

Table 2
Specifications of structural columns and beams used in B-44 and B-60 buildings.

B-60			
Floor level	Column	Beam Long direction	Beam Short direction
1–10	CR 50 × 3 × 40 × 3	W 24 × 207	W 27 × 281
11–20	CR 50 × 2 × 40 × 2	W 24 × 207	W 27 × 281
21–30	CR 50 × 2 × 30 × 2	W 24 × 162	W 24 × 279
31–40	CR 30 × 3 × 20 × 3	W 24 × 162	W 24 × 279
41–50	CR 30 × 2 × 20 × 2	W 24 × 104	W 27 × 146
51–60	CR 30 × 1 × 20 × 1	W 24 × 104	W 27 × 146
B-44			
1–10	CR 50 × 3 × 40 × 3	W 18 × 119	W 24 × 370
11–22	CR 50 × 3 × 30 × 3	W 18 × 119	W 24 × 370
23–33	CR 50 × 2 × 30 × 2	W 18 × 119	W 24 × 250
34–44	CR 50 × 2 × 20 × 2	W 18 × 119	W 24 × 250

Table 3
Limiting values of inter-story drift in non-structural components from standard building codes.

	Structural/Non-structural component	***IDR* (%)**	**Adopted from**
1	Exterior walls with brittle finishes	0.42	International Building Code (IBC) (2003)
	Exterior walls with flexible finishes	0.83	
	Aluminum panels used in walls of sunroom additions	1.67	
	Structural members supporting glass unit masonry	0.17	
2	Drift of walls and frames to prevent damage to non-structural components	0.17–0.25	ASCE 07 (2016)
3	Roof drift with seismic loads	1.00	Building Research Association of New Zealand (1999)
	Walls, face loading	0.50	
	Walls, in-plane loading	0.20	
	Facades/ curtain wall	0.67	
	Other linings	0.40	
4	In-plane loading of walls and masonry and plaster	0.20	Cooney and King (1988)
	Moveable partitions	0.20	
	In-plane loads on facades and curtain walls	0.67	
5	Interior finishes	0.20	National Building Code of Canada (2015)

$\lambda_L = 1.2158, \lambda_M = 0.6007$

The comparison between flutter derivatives calculated from RFCs calculated above with that of the experimental results presented by Sauder and Sarkar [46] for the 3DOF system are shown in Figs. 4 to 6 for the vertical, lateral, and torsional motions, respectively. These values for the 2DOF system are shown in Figs. 7 to 9. The RFC's themselves are not the same as Sauder and Sarkar [49] as the algorithms are different. However, the comparisons show a good match between the derivatives in most of the cases. The terms associated with the damping coefficients match accurately. The flutter derivatives showing deviations from the original are H_4^*, H_6^*, P_4^*, P_6^*, A_4^* and A_6^*. They are the frequency-dependent terms and hence the discrepancies may be ignored.

As shown in this section the RFA is critical in the development of a detailed wind load model that captures the building-environment interactions in the time domain. The RFCs presented here from the RFA can be used to derive flutter derivatives and vice versa for buildings with the same aspect ratio of 5:1. The RFCs can be used to calculate the self-excited loads acting on the structure in time domain. For buildings or structures with a different aspect ratio, the flutter derivatives or rational function approximations would have to be obtained from the free vibration/ forced vibration tests of the section model in a wind tunnel or in the absence of test results by approximating the flutter derivatives based on quasi-steady formulations. The flutter derivatives can then be used to derive the RFAs in time domain. The case studies of the two tall buildings presented further in this study have an aspect ratio of 1.5:1. The flutter derivatives obtained from wind tunnel tests by Hou and Sarkar [34] and quasi-steady formulations given by equations (23) to (30) were used in the derivation of RFAs in the case studies. The RFAs used in the study are shown here from (c1) to (c3). The RFAs for higher reduced velocities than those given in Fig. 3 are also assumed to be the same instead of using extrapolation.

Table 4
Limiting Peak accelerations for Occupant Comfort reported by Goto (1983).

Interruption to Activity	**Threshold Acceleration (m/s^2)**
Perception Threshold	0.05
Psychological and task performance	0.4
Walking	0.5–0.7
Safety	0.8

$$A_0 = \begin{bmatrix} -2.658 & 0.000 & 7.100 \\ 0.000 & 0.296 & -0.760 \\ 0.000 & 0.000 & 0.262 \end{bmatrix} \quad \text{(c1)}$$

$$A_1 = \begin{bmatrix} 1.030 & 0.000 & -7.100 \\ -0.760 & -1.138 & 0.190 \\ -0.034 & 0.000 & -2.600 \end{bmatrix} \quad \text{(c2)}$$

$$A_2 = \begin{bmatrix} 3.020 & 0.000 & 0.000 \\ 0.000 & -0.282 & 0.000 \\ 0.000 & 0.000 & -0.190 \end{bmatrix} \quad \text{(c3)}$$

$\lambda_L = 1.186, \lambda_D = 0.865$ and $\lambda_M = 0.500$

3. Development of a nonlinear structural model

Two tall buildings with standard CAARC (Commonwealth Advisory Aeronautical Research Council) configurations are designed for the purpose of this study. The buildings are 210 m and 160 m tall with 60 and 44 floor levels, respectively. They both have a plan aspect ratio (B/D) of 1.5:1. Buildings with two different heights are considered to study the amplification of structural response due self-excited forces and the effects on occupant comfort as buildings grow taller. The buildings will be referenced for the remainder of the paper as B-60 and B-44 representing the number of floor levels. The steel frames are composed of beams made from wide flanged I-sections and columns of cross rectangular sections built-up with wide flanged I sections. The steel beams in the frame have a span of 8 m each with 6 spans along the longer direction and 4 spans in the perpendicular direction. The 3-D views of both the buildings along with the plan view is shown in Fig. 10 (a) to 10(c). The buildings were designed under static loads based on the provisions of AISC 360 [50] and ASCE 7 [16] for a design wind speed of 58 m/s for Miami Dade county in Florida. The static analysis, and design was conducted in SAP2000 [51] and frame sections were chosen to satisfy the code-specific structural design requirements.

To conduct the nonlinear time-history analysis of the whole time-history of the wind events, the structure was modeled in OpenSees [52]. OpenSees is a software framework for developing applications to simulate the performance of structural and geotechnical systems subjected to earthquakes. Hence, the software is also capable of performing nonlinear time-history analysis under wind loads. The design of tall buildings under dynamic loads introduces a series of challenges that need to be met through consideration of scientific, engineering and regulatory issues specific to the modeling, analysis and acceptance criteria appropriate for these unique structural systems. ATC-72 [53], provides guidance on selection of component model types, modeling of deterioration, capture of P-Delta effects, consideration of damping, quantification of expected properties and consideration of uncertainty.

The materials and elements available in the OpenSees library are used in the development of the model. The nodes are assigned based on

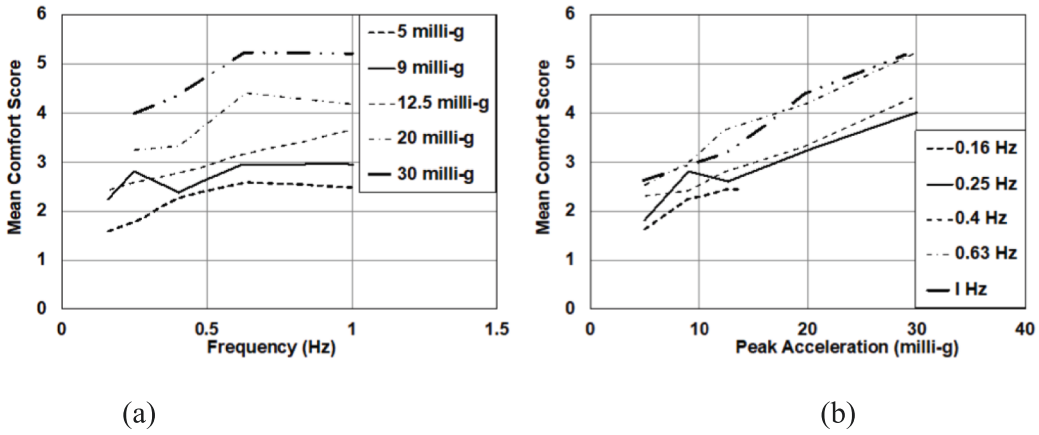

Fig. 12. Comfort score curves given by Michaels 2013 (a) function of frequency and (b) function of peak acceleration.

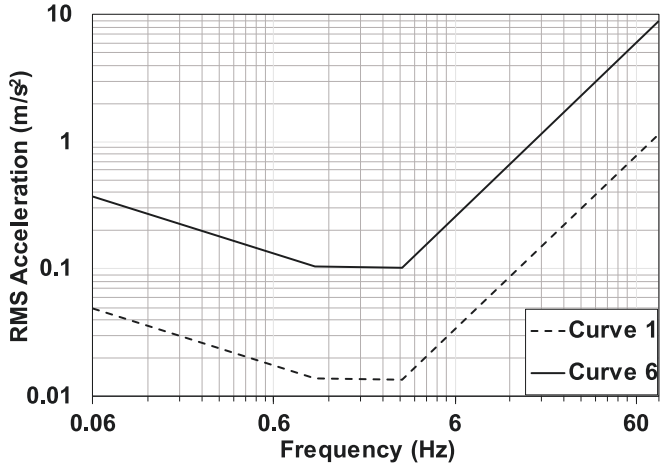

Fig. 13. Threshold acceleration curves given by Irwin (1978).

the respective story heights and frame spacing. The beam-column elements are modeled using force-based element available in OpenSees library. Force-based elements (FBE) are based on distributed plasticity models that allow for spread of plasticity along the element. These elements allow yielding to occur anywhere along the element. A typical FBE used in the model is shown in Fig. 11.

The force-based method is based on interpolation functions for the internal forces. The force interpolation functions strictly enforce the exact force distribution through the element. FBE was preferred over the displacement-based element (DBE). The reason for this is that the FBE satisfies strong form of equilibrium as the forces are exact whereas in DBE equilibrium is achieved by averaging the values at each integration point. It does not satisfy the force equilibrium at any arbitrary point in the element but rather in a global sense i.e., it satisfies weak equilibrium. Both the methods are vulnerable to integration errors. However, the accuracy of solution in an FBE can be improved by increasing the number of integration points whereas in a DBE increasing the number of elements is the only way to attain the same level of accuracy. Increasing the number of elements for each structural member would results in higher number of nodes and hence increase in computational effort, which would make the analysis more cumbersome considering the length of the time-history of wind loads. The default Gauss-Lobatto integration is assumed for evaluating the responses and the number of integration points are set as 6 along the length of the element.

The nodes in each floor are assigned to a diaphragm using the rigid diaphragm function. The beams and columns of the frame is composed entirely of structural steel members. The material from the OpenSees library, Steel02 (Giuffre-Menegotto-Pinto Model) is used to model the members which has a yield stress, $F_y = 345$ MPa and modulus of elasticity, $E = 2 \times 10^5$ MPa with isotropic hardening properties. The parameters used in the material definition to transition from elastic region to post yield behavior includes a strain hardening ratio of 0.05, $R_0 = 15$, $c_{R1} = 0.925$, and $c_{R2} = 0.15$. The structural damping is set to 2 percent and Rayleigh damping is used.

The frame is composed of rectangular cross sections built-up from wide flanged I-sections for the columns and wide flanged I-sections for the beams. The various sections used in the buildings are listed in Table 2. The beams are made from standard wide-flange sections available in AISC 360 [50] and the column dimensions are given in inches and represent the column depth, thickness, and width. The column and beams section dimensions are gradually reduced with increasing story levels. This is expected because the loads acting on the members of higher floor levels are lower than those on lower levels. The sections are modeled using the fiber section function inbuilt in the OpenSees library. This enables modeling each section as a group of fibers with a specific uniaxial material, area and location. The number of fibers along the width and thickness dimensions are taken as 6 and 1, respectively. The mass of the structural components is defined in terms of mass density and is assigned with the element definitions. The additional loads acting on the structure includes the superimposed dead loads and live loads along with the wind forces. The dead and live loads considered in the design were chosen from ASCE-07 [16] conforming to the requirements of an office building. The dead and live loads are applied on the model as uniformly distributed floor loads. The wind loads consisting of turbulent buffeting forces and self-excited forces are applied to the nodes on the surface along and across the direction of wind flow.

Table 5
Threshold accelerations given by ISO 6897 (1984) based on functionality of buildings.

General Purpose Buildings		Special Purpose Buildings		Offshore Structures	
Frequency (Hz)	Limiting Acceleration (m/s^2)	Frequency (Hz)	Limiting Acceleration (m/s^2)	Frequency (Hz)	Limiting Acceleration (m/s^2)
0.067	0.081	0.067	0.051	0.067	0.485
1.000	0.026	1.000	0.014	1.000	0.156

Table 6
Threshold accelerations given by ISO 6897 (1984) for short duration wind events based on the functionality of buildings.

Center Frequency (Hz)	RMS acceleration (m/s^2)			
	General-purpose buildings	Offshore structures	Special purpose buildings	
			Lower Threshold	Mean Threshold
0.063	0.0815	0.489	0.01260	0.0504
0.080	0.0735	0.441	0.01140	0.0450
0.1	0.0670	0.400	0.01030	0.0409
0.125	0.0610	0.366	0.00920	0.0370
0.160	0.0550	0.330	0.00830	0.0330
0.200	0.0500	0.300	0.00750	0.0300
0.250	0.0460	0.276	0.00690	0.0270
0.315	0.0418	0.250	0.00610	0.0240
0.400	0.0379	0.228	0.00550	0.0219
0.500	0.0345	0.207	0.00490	0.0198
0.630	0.0315	0.189	0.00445	0.0178
0.800	0.0285	0.167	0.00398	0.0159
1.000	0.0260	0.156	0.00360	0.0144

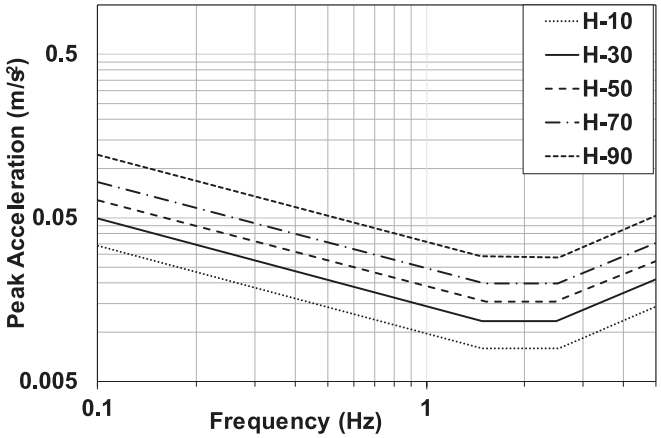

Fig. 14. Threshold accelerations given by AIJ-GBV [84] as a function of frequency.

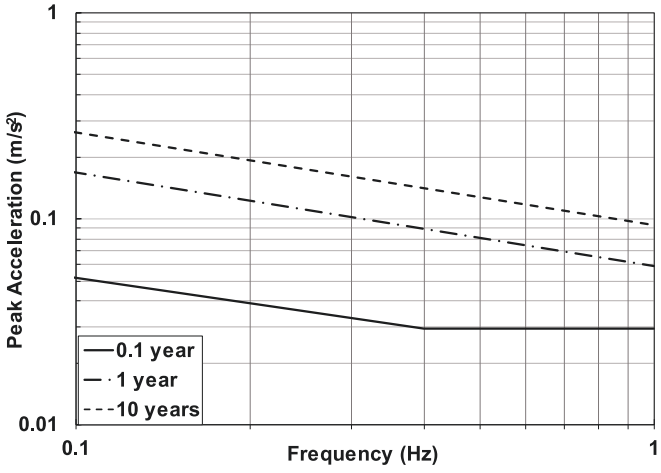

Fig. 15. Threshold accelerations given by ASCE Pre-standard (2019) as a function of frequency.

4. Nonlinear time-history analysis under wind loads

To evaluate the different engineering demand parameters associated with different levels of wind loading, the two case study buildings: B-44 and B-60 are subjected to varying wind speeds ranging from 18 m/s to 67 m/s. The buffeting loads and self-excited wind loads are applied in the along-wind, across-wind and torsional directions. The wind loads are applied at zero-degree angle of incidence. The turbulent (buffeting) load time histories are generated based on the algorithm proposed by Deodatis [54]. The process involves generating the $[n \times n]$ Cross Spectral Density Matrix, where n denotes the number of variates or the number of time histories to be generated. The elements of the matrix are derived based on Power Spectral Density Functions (PSDF) given by Kaimal et al. [55]. The cross spectral density matrix is then decomposed using the Cholesky's method. The elements along the diagonal of the lower triangular matrix obtained after decomposition are real and the off-diagonal terms are complex functions. The stochastic process simulations are then performed using Fast Fourier Transforms (FFT). The obtained turbulent time histories are converted to buffeting loads. The expressions for buffeting loads based on QST are adopted here, where for typical turbulence intensities present in the atmosphere it may be assumed that the squares of the velocity fluctuations are negligible with respect to the square of the mean wind speed and that the load coefficients are independent of the frequency in the range considered. The equations for the buffeting loads in QST are given by Equations (31) to (33).

$$D_B(t) = \frac{1}{2}\rho U(z)^2 Bh\left[C_D\left(1+2\frac{u(z,t)}{U(z)}\right)+\left(\frac{dC_D}{d\theta}-C_L\right)\frac{v(z,t)}{U(z)}\right] \tag{31}$$

$$L_B(t) = \frac{1}{2}\rho U(z)^2 Bh\left[C_L\left(1+2\frac{u(z,t)}{U(z)}\right)+\left(\frac{dC_L}{d\theta}+C_D\right)\frac{v(z,t)}{U(z)}\right] \tag{32}$$

$$M_B(t) = \frac{1}{2}\rho U(z)^2 B^2 h\left[C_M\left(1+2\frac{u(z,t)}{U(z)}\right)+\left(\frac{dC_M}{d\theta}\right)\frac{v(z,t)}{U(z)}\right] \tag{33}$$

where h is the mean story height of the building at height z, C_D, C_L and C_M are the aerodynamic load coefficients for drag, lift and torsional moment, respectively, and $\frac{dC_D}{d\theta}$, $\frac{dC_L}{d\theta}$ and $\frac{dC_M}{d\theta}$ are the corresponding derivatives of these coefficients with respect to angle of attack (θ), all of which are obtained from the wind tunnel tests. These coefficients and their derivatives are dependent on the angle of attack, θ. The aerodynamic load coefficients in Equations (31) to (33) are obtained from wind tunnel tests on scaled models of cross-section of the building. Hence, the aerodynamic load coefficients and their derivatives used in the wind load model are assumed to be constant over the height of the building. This limitation can be addressed by extracting the aerodynamic load coefficients from wind tunnel tests on scaled models of buildings. The buffeting loads in the along-wind, across-wind and torsional directions are considered in this study. The self-excited wind loads were calculated based on the numerical formulations presented in section 2. The varying angles of attack of wind speeds are not considered in this study as directionality analysis is not part of the scope of this study, however, in reality the winds can act from multiple angles. As such, the directionality factor given by ASCE-07 [16] for the calculation of design wind speed is taken as 1. The buildings were analyzed under two conditions of wind actions: Turbulent/buffeting loads only, turbulent and self-excited forces to represent the effects that the more complex but accurate wind load models including self-excited forces. The lower end wind speeds of 18 m/s to 36 m/s was included in the analysis to particularly observe occupant comfort under wind speeds with smaller return periods. Structural damage is not expected to occur at these wind speeds as the buildings are designed for a much higher design wind speed.

B-44 and B-60 were analyzed for gravity and wind actions using nonlinear dynamic time-history analysis in OpenSees. The buildings were analyzed for 30-minute duration wind loads with a time step of 0.1 s. The building responses recorded were nodal displacements and accelerations and member forces in beams and columns. The results from the time-history analysis were observed to show much higher responses

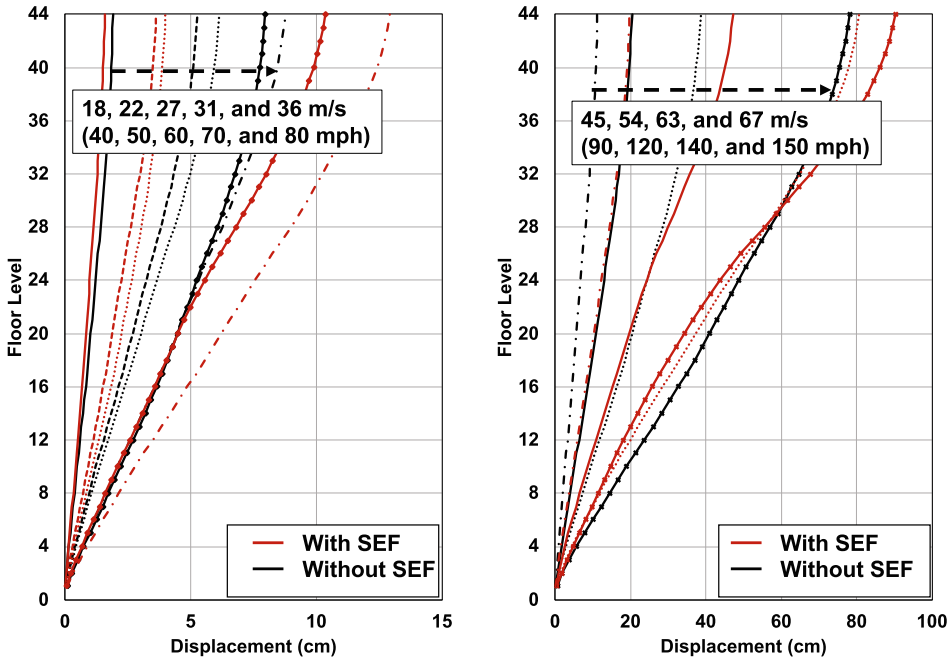

Fig. 16. Comparison of peak displacements for B-44 in the across-wind direction with bufetting and self-excited forces (With SEF) and without self-excited forces (Without SEF) for wind speeds (a) 18–45 m/s and (b) 54–67 m/s.

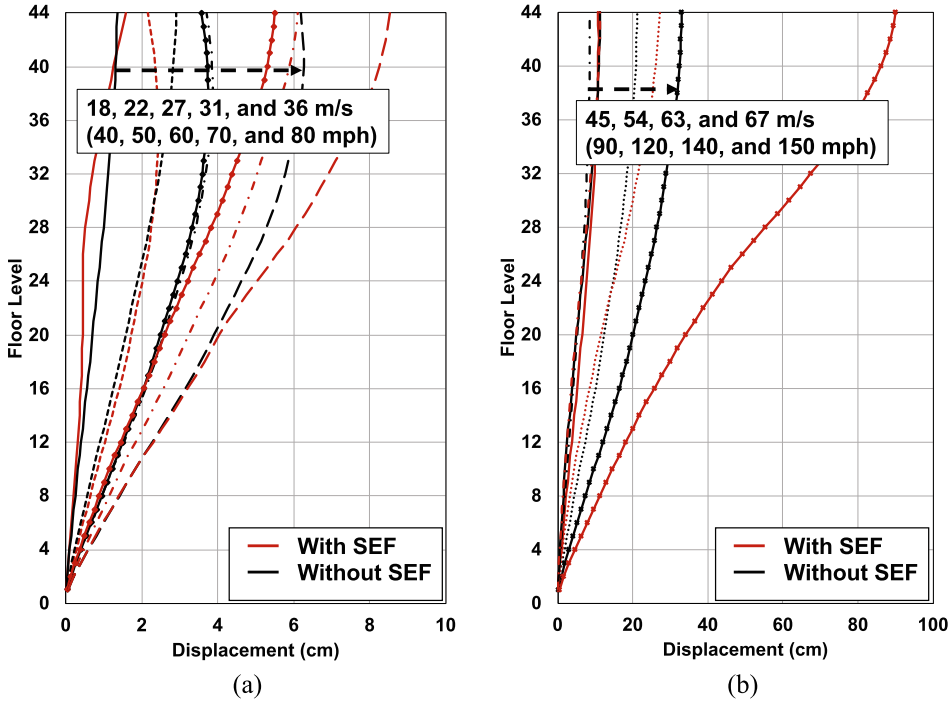

Fig. 17. Comparison of peak displacements for B-44 in the along-wind direction with bufetting and self-excited forces (With SEF) and without self-excited forces (Without SEF) for wind speeds (a) 18–45 m/s and (b) 54–67 m/s.

at the beginning of the analyses because of the sudden loads acting on the structure. Those results were filtered out when analyzing and reporting the time-history responses used in the study. The initial peaks were found to subside and stabilize for all the responses (i.e., displacements, accelerations, and member forces) after the first 150 steps equivalent to 15 s of wind loads and hence only the data beyond the 150th time step was used for the results presented in the study.

5. Performance objectives associated with PBWD

The decision variables (*DV*) in PBWD are chosen to assess the performance of structures. The *DV*s chosen in this study are the structural displacements, inter-story drift ratios (*IDR*) and floor accelerations. The displacements and *IDR* are used to identify the propagation of structural and non-structural damage and the accelerations are used to evaluate

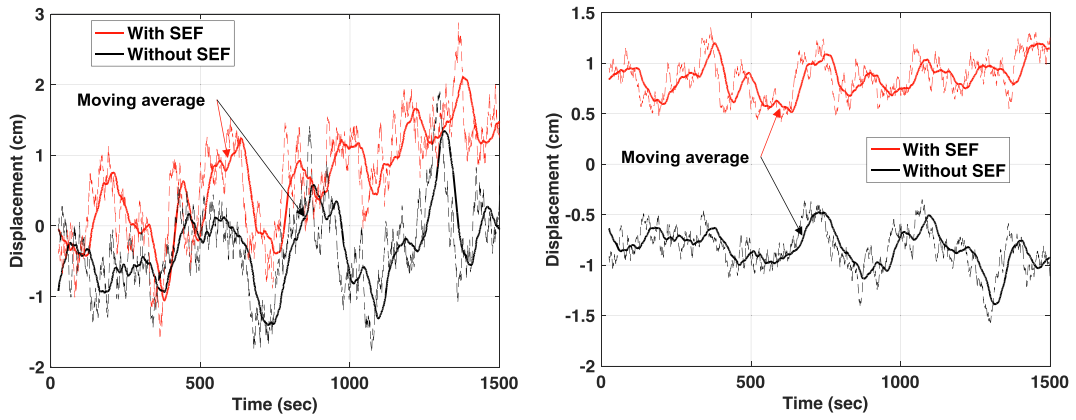

Fig. 18. Peak displacement (at the top of building) time-history of B-44 at 18 m/s showing lower responses under loading with self-excited forces compared with those without, (a) acrosswind and (b) along-wind responses.

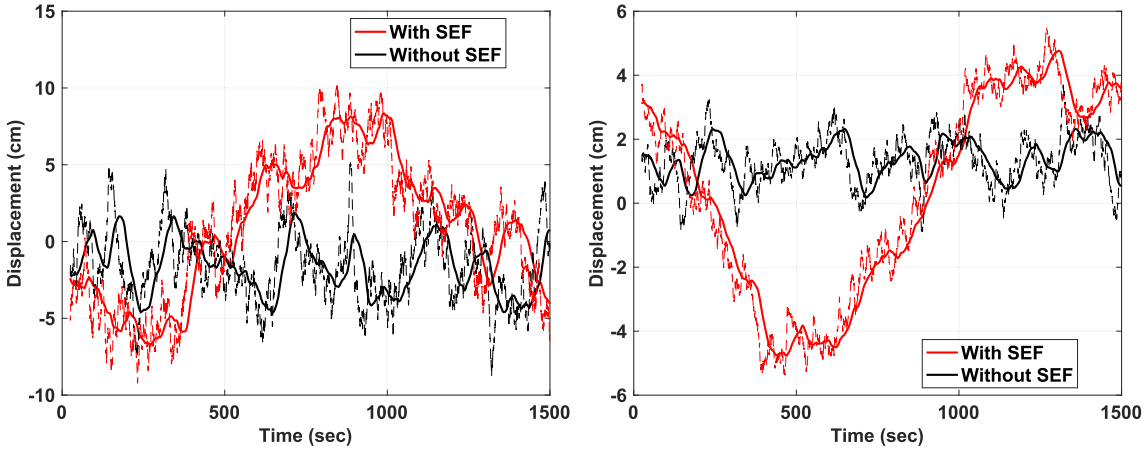

Fig. 19. Peak displacement (at the top of building) time-history of B-44 at 31 m/s showing higher responses under loading with self-excited forces compared with those without, (a) acrosswind and (b) along-wind responses.

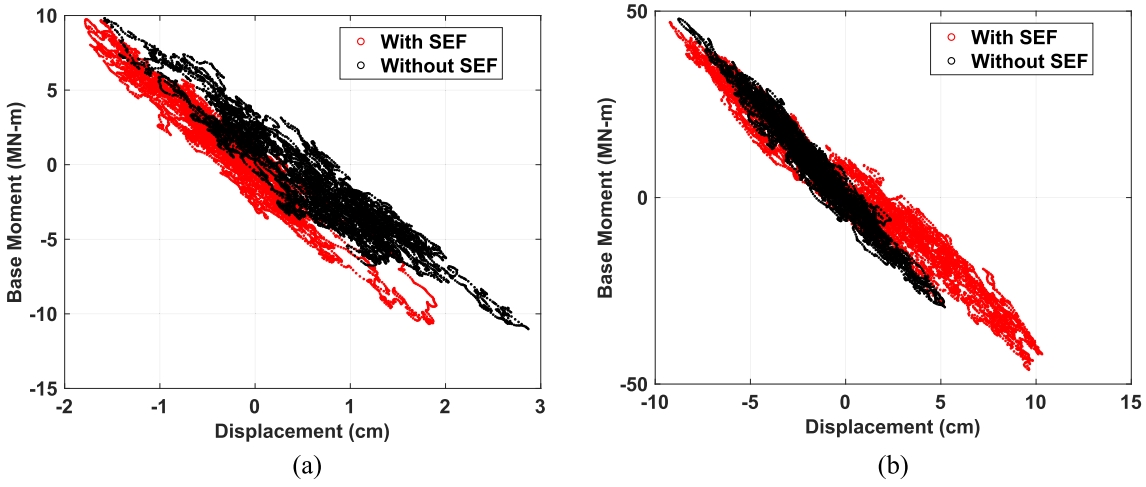

Fig. 20. Base Moment-Peak displacement relationships of B-44 at (a) 18 m/s and (b) 31 m/s showing comparison of building responses under the action of self-excited forces.

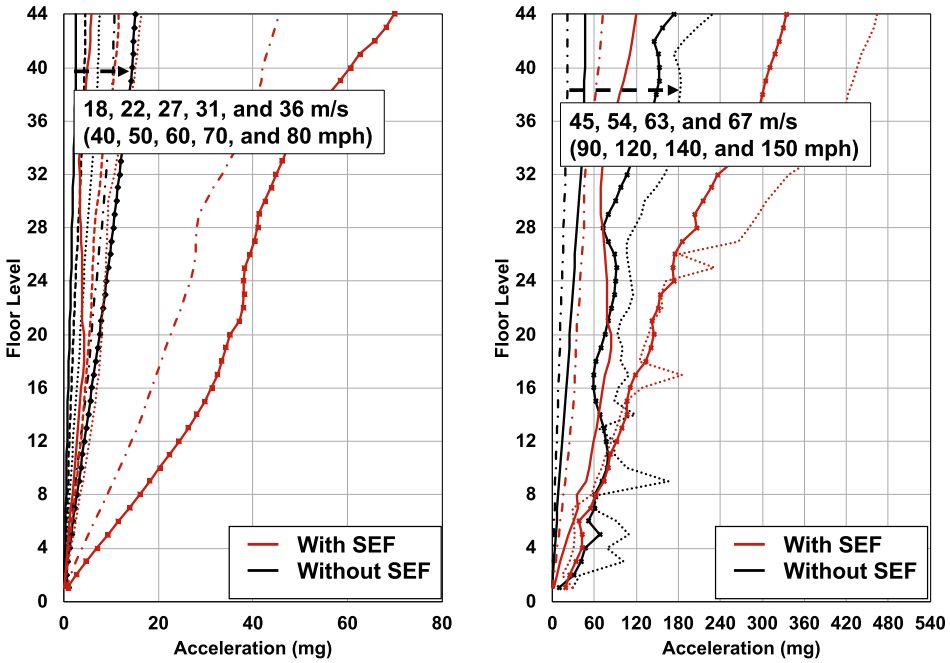

Fig. 21. Comparison of peak accelerations for B-44 in the across-wind direction with bufetting and self-excited forces (With SEF) and without self-excited forces (Without SEF) for wind speeds (a) 18 – 40 m/s and (b) 54–67 m/s.

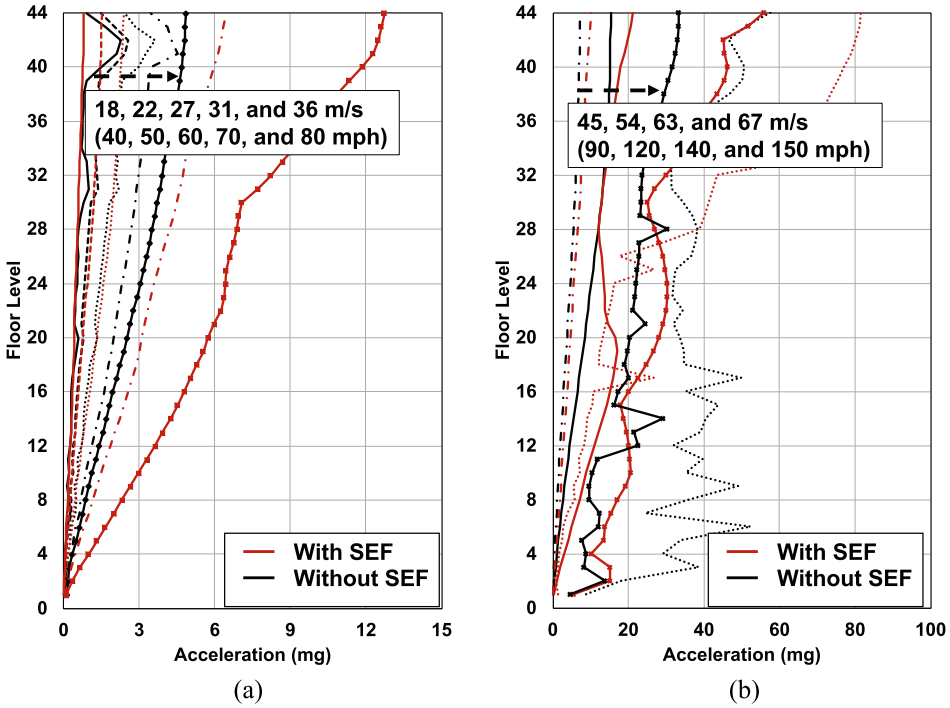

Fig. 22. Comparison of peak accelerations for B-44 in the along-wind direction with bufetting and self-excited forces (With SEF) and without self-excited forces (Without SEF) for wind speeds (a) 18 – 40 m/s and (b) 54–67 m/s.

the human perception of motion or occupant comfort in the building. Such displacements and *IDR* in tall buildings can be accurately predicted using numerical simulations or data driven techniques such as [56–59]. The standard building codes specify the limiting *IDR* or displacements based on the failure of the building and are not specific to the various structural and non-structural components within the building. The drift limits specified in various research studies and international standards for structural and non-structural components are summarized in Table 3. The forces within the structural beams and columns are recorded to pinpoint the locations of member failure. The recording is done at every time step to also identify the failure time step. This can provide insights on the influence of duration of loading on the amplification of structural responses. Considering that occupation comfort is not a performance objective of interest within the PBSD but majorly

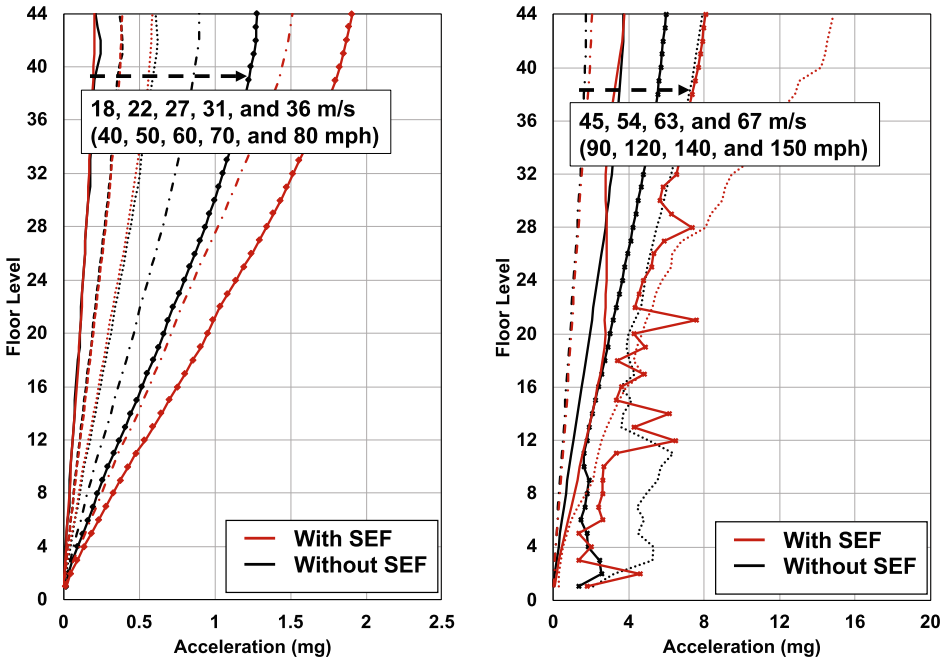

Fig. 23. Comparison of RMS accelerations for B-44 in the along-wind direction with bufetting and self-excited forces (With SEF) and without self-excited forces (Without SEF) for wind speeds (a) 18 – 40 m/s and (b) 54–67 m/s.

impacts the design assumptions in the PBWD, an extensive review of available thresholds for occupant comfort in tall buildings under dynamic wind actions has been collected and will be used for the PBWD framework. The review covers the significant experimental and analytical research conducted over the years on evaluating occupant comfort and discusses the available design specifications implemented in International standards.

5.1. Review of occupant comfort thresholds

Studying human perceptions maybe done through field experiments and surveys, shake table tests, and field experiments on artificially excited buildings. Multiple researchers [60–65] have conducted numerous field experiments and surveys on tall buildings to examine their habitability under various wind conditions. The surveys were prepared accounting for motion, noise, and visual observations. Hansen et al. [60] gave a limiting RMS acceleration of 0.005 g for a 6-year return period wind event studying the habitability of tall buildings. RMS accelerations can be a good representation of the sensations experienced by occupants in sustained events, as the duration and number of cycles of motion that occur above a threshold value may be more significant for occupants than an occasional high peak. However, Melbourne and Palmer [61] stated that using RMS accelerations could significantly overestimate the building motion because the crosswind force spectrum at the peak departs from a normal distribution, thereby lowering the peak factor. Goto [62] presented peak acceleration limits (Table 4) based on survey results of occupants investigating motion sickness in higher floors of tall buildings. Further, studies by Lee [63], Chang [64] and Denoon et al. [65,66] also expressed threshold limits in terms of mean maximum accelerations on a building that experienced motion during a windstorm.

Major field experiments by Correa et al. [67,68] on tall buildings aimed to correlate full-scale monitoring to building performance in terms of lateral and torsional accelerations to occupant perceptions. The simulated environments though not ideal can provide reasonable estimates of tenant comfort levels in tall buildings where ideal investigations are not possible. Another study published by Lamb et al. [69] investigated occupant comfort through a human survey in the tall buildings of Wellington, New Zealand, under wind and earthquake vibrations. The survey also contained the motion sickness susceptibility questionnaire prepared by Golding [70]. These studies showed that people susceptible to motion sickness expressed a preference for the lower floors of the building and those constrained in higher floors experienced heightened symptoms of motion sickness.

An early study focused on evaluating occupant comfort using a motion simulator was done by Irwin [71] and based on the response of the test subjects, RMS acceleration threshold limits were recommended over a wide range of frequencies between 0.01 and 10 Hz. Michaels [72] developed logistic regression models to predict human behavior under wind events and investigated the effects of frequency, acceleration magnitude, duration of vibration and cultural factors on occupant comfort. The results from the study are shown in Fig. 12. Test subjects felt increasing discomfort with increasing accelerations and higher frequencies. This agrees with all other major studies conducted on evaluating occupant comfort. Other significant studies on occupant comfort using motion simulators were conducted by [73–77]. Artificially exciting buildings through full-scale experiments is perhaps the most accurate method to understand motion perception. Notable studies by artificially exciting buildings were done by Morris et al. [78] and Bouncer et al. [79].

5.2. Design standards for occupant comfort

Irwin [80] stressed the need for standard design recommendations for habitability or occupant comfort in addition to strength and serviceability criteria. Based on the data from studies, he identified that accelerations controlled human perception in low frequency vibrations (up to 1.9 Hz). The higher frequency motions are velocity and displacement controlled. He developed a curve for the upper limit of accelerations in office or housing buildings. RMS acceleration was chosen as the design criteria and was averaged over the worst 10 min for windstorms with a return period of 5 years. Irwin [81] published

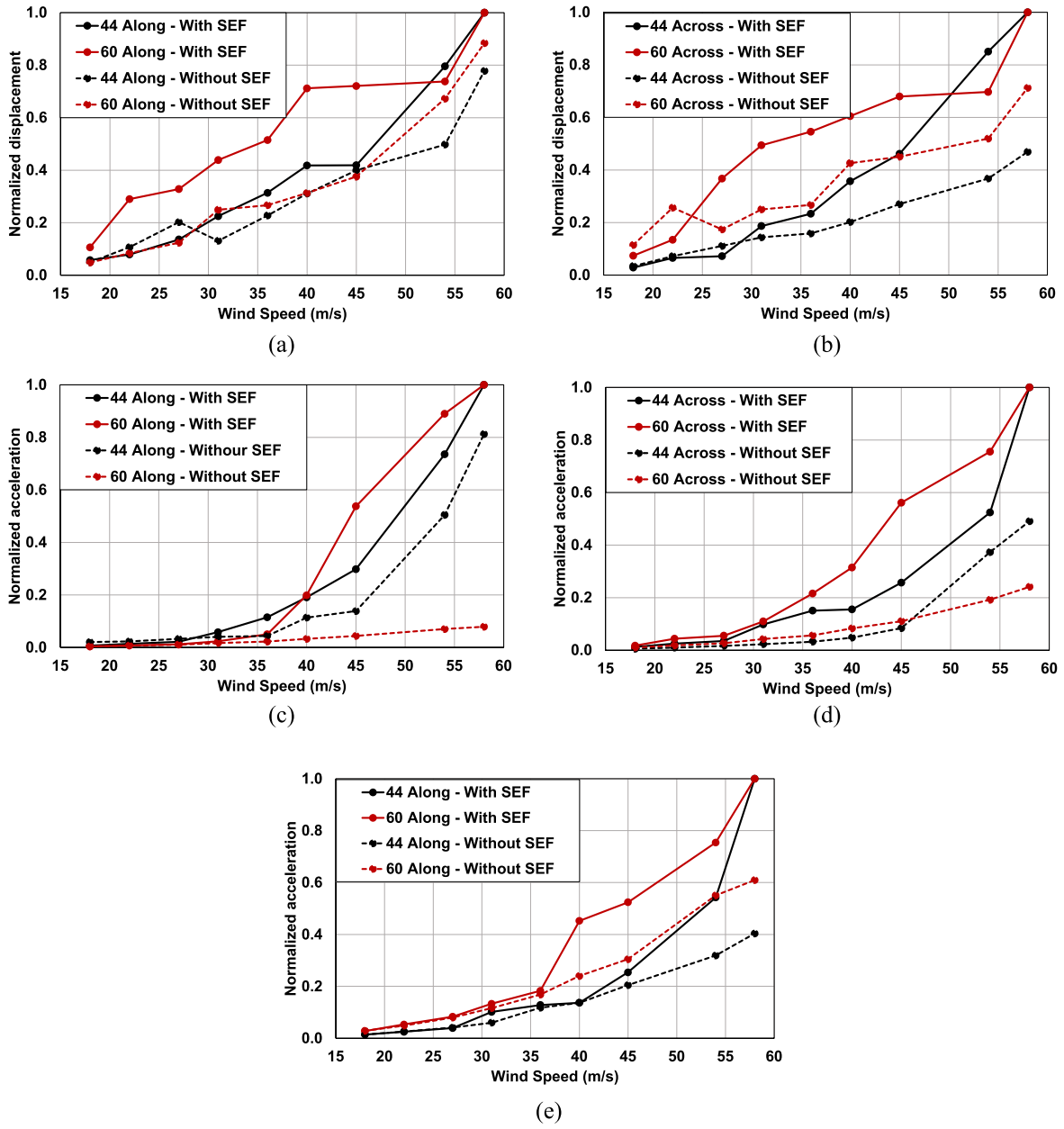

Fig. 24. Comparison of structural responses: displacements in the (a) along-wind direction and (b) across-wind direction, accelerations in the (c) along-wind direction and (d) across-wind direction and (e) RMS accelerations in the along wind direction.

Table 7
Percentage perception experienced by occupants of B-44 based on the specifications by AIJ [84].

Wind Speed (m/s)	1-yr Wind Speed (m/s)	Along-wind peak acceleration (m/s^2, Without SEF)	Highest % Perception	Along-wind peak acceleration (m/s^2, With SEF)	Highest % Perception	Across-wind peak acceleration (m/s^2, Without SEF)	Highest % Perception	Across-wind peak acceleration (m/s^2, With SEF)	Highest % Perception
31	18	**0.022**	H-10	**0.008**	H-10	**0.025**	H-10	**0.057**	H-70
36	22	**0.025**	H-30	**0.015**	H-10	**0.045**	H-50	**0.114**	H-90
45	27	**0.036**	H-30	**0.023**	H-30	**0.074**	H-70	**0.160**	H-90
54	31	**0.044**	H-50	**0.063**	H-70	**0.105**	H-90	**0.447**	H-90
58	36	**0.048**	H-50	**0.125**	H-90	**0.148**	H-90	**0.685**	H-90
67	40	**0.123**	H-90	**0.208**	H-90	**0.217**	H-90	**0.707**	H-90

expanded recommendations for limiting accelerations based on occupant comfort. The recommendations were made for buildings, bridges and other offshore structures and later served as the major foundation for development of ISO 6897 [82]. The maximum magnitudes of horizontal motion of buildings are given by curve 1 in Fig. 13 while curve 6 gives the thresholds for offshore structures and bridges.

ISO 6897 [82] was the first international standard developed for evaluation of occupant comfort for fixed structures such as buildings and

Table 8
Percentage perception experienced by occupants of B-60 based on the specifications by AIJ [84].

Wind Speed (m/s)	1-yr Wind Speed (m/s)	Along-wind peak acceleration (m/s^2, Without SEF)	Highest % Perception	Along-wind peak acceleration (m/s^2, With SEF)	Highest % Perception	Across-wind peak acceleration (m/s^2, Without SEF)	Highest % Perception	Across-wind peak acceleration (m/s^2, With SEF)	Highest % Perception
31	18	**0.028**	H-10	**0.028**	H-10	**0.080**	H-90	**0.137**	H-90
36	22	**0.049**	H-30	**0.052**	H-30	**0.143**	H-90	**0.344**	H-90
45	27	**0.072**	H-90	**0.080**	H-90	**0.209**	H-90	**0.434**	H-90
54	31	**0.115**	H-90	**0.161**	H-90	**0.333**	H-90	**0.859**	H-90
58	36	**0.152**	H-90	**0.344**	H-90	**0.441**	H-90	**1.692**	H-90
67	40	**0.224**	H-90	**1.359**	H-90	**0.653**	H-90	**2.471**	H-90

offshore structures subjected to low frequency vibrations (0.063 to 1 Hz). The recommendations given by Irwin [81] served as a major reference in developing the code and uses the same criteria for the selection of acceptable complaint levels, return period and averaging intervals. The code continues to be used today without any revisions. Since this study is on tall buildings, only the provisions for buildings will be discussed here. The code gives limiting horizontal motions in terms of RMS accelerations corresponding to discrete frequencies of vibrations. The limiting accelerations given by the code for buildings based on their functionality are given in Table 5. The thresholds corresponding to the center frequency of one-third octave band are given in Table 6 to be used for short duration vibrations less than 10 min. Melbourne and Cheung [83] modified the threshold limits given in ISO 6897 in terms of peak accelerations with appropriate multiplication factors to convert RMS accelerations to peak accelerations.

Based on the evolution of studies on habitability and occupant comfort, the Architectural Institute of Japan Guidelines for Building Vibration (AIJ-GBV) [84] was revised and published in 2004. AIJ-GBV [84] covered wind-induced vibrations up to 5 Hz. This was to account for the vibrations experienced by low-rise buildings under wind loads. Fig. 14 shows the threshold curves given by the standard. Each curve has the nomenclature corresponding to the percentage of perception probability. For example, curve H-90 means that 90% of the people can perceive motion at the given threshold. Since the curves are given in terms of perception probability, it is up to the designers and building owners to choose the curve according to their requirements. The code itself does not impose regulations on the choice of curves. The Pre-standard for Performance-Based Wind Design published by ASCE in 2019, provides acceptance criteria for occupant comfort based on peak acceleration limits. The criteria are set based on the recommendations given in ISO 6897, AIJ 2004, ISO 2007 and several significant research cited in this section. The pre-standard gives acceleration limits for wind speeds with return periods of 0.1, 1 and 10 years. Short return periods are given to account for frequent vibrations resulting from vortex shedding. The comfort criteria for office occupancy is given by Fig. 15.

The studies discussed here prove there is no universal consensus on the limit states of acceleration for occupant comfort. Peak and RMS values have both been widely used in studies and in the development of design standards to categorize occupant comfort. It appears that peak acceleration is the engineering demand parameter mostly adopted by the industry while the RMS values are more utilized by the research community. In the absence of a comprehensive document, it is advisable to decide the limiting accelerations by considering both the peak and RMS accelerations in a building. Hence, In this study both the RMS and peak values of accelerations presented in the codes are used in the evaluation and discussions for occupant comfort.

6. Results and discussion

6.1. Case study 1: B-44

The results from the analyses of the 44-story building are presented in Figs. 16 to 23. Figs. 16 and 17 shows the comparison of peak displacements along the height of the building in the across-wind and along wind directions. Comparisons are made by increasing wind speeds and more importantly on the effects of application of self-excited forces (SEF) in addition to buffeting forces. The figures show a reduction in structural displacements due to addition of self-excited forces for lower wind speeds (less than 27 m/s) and increasing displacements for higher wind speeds. This is because the aeroelastic damping adds to the structural damping at lower wind speeds due to the positive variation of aeroelastic coefficients in this range. But at the higher wind speeds, where the H^* flutter derivatives shift to positive values (as seen in Fig. 3 (a)), the negative aerodynamic damping reduces the structural damping thereby amplifying the responses as seen in the figures. The significant amplification of displacements at 67 m/s is due to the yielding of multiple columns and the highly nonlinear response of the structure at high wind speeds upon addition of self-excited forces. The figure also shows lower responses with SEF than without SEF at 67 m/s upto 29th story. Such modification of aerodynamic behavior is only observed in the across-wind response and it can be explained as the increase in structural damping due to the addition of aeroelastic coefficients at such high wind speeds. The flutter derivatives given in Fig. 3 are only available for a limited range of wind speeds and the derivatives are assumed the same for higher wind speeds. Hence, additional experimental studies maybe conducted to validate such structural response in future. This also shows the high amplification of responses due to self-excited forces and proves the importance of considering its effects to fully understand the interaction of structures and the wind environment.

The time-history variation of displacements in the across-wind and along-wind directions at 18 m/s and 31 m/s are shown in Figs. 18 and 19, respectively. The figures show significant reduction in across-wind displacements influenced by the variation of H^* coefficients at 18 m/s increasing the aeroelastic stiffness. 31 m/s is chosen as the wind speed for Fig. 19 to show the responses immediately over the cross-over wind speed and here the responses considering the self-excited forces are visibly higher than those without. Fig. 20 also shows similar behavior with the base moment and peak displacement relationship at 18 m/s and 31 m/s.

The acceleration responses for B-44 are shown in Figs. 21 to 23 for the same range of wind speeds. The figures show very different behavior in accelerations at high wind speeds when compared to displacement responses in terms of nonlinearity. The nonlinearity experienced by the building can be seen from the across-wind and along-wind acceleration response curves in Figs. 21 and 22. Highly nonlinear behavior is observed for wind speeds greater than ~ 60 m/s, which is higher than the design wind speed of 58 m/s. The figures also show higher nonlinearity without SEF in the lower floor levels than at the peak floors consistent with the displacement responses in Fig. 18. In the case of accelerations, it can be seen that the responses with SEF is lower than those without SEF for wind speeds up to 31 m/s in the along-wind direction only. The RMS accelerations in Fig. 23 similarly shows the nonlinearity at higher wind speeds. From the low accelerations reported in RMS plots, the peak accelerations reported earlier are recorded for very short durations and does not represent the structural response under sustained durations of loading. From the literature review

Table 9
Fragility groups, damage states and drift ratio limits obtained from FEMA database.

Structural/Non-structural Components	Damage Parameter	Damage States	Description	Median; Dispersion
Welded column splices	Story drift ratio	DS1/DS2 DS3	**DS1**: Ductile fracture of the groove weld flange splice. Damage in field is either obscured or deemed to not warrant repair. No repair conducted. **DS2**: Ductile fracture of the groove weld flange splice **DS3**: DS1 followed by complete failure of the web splice plate and dislocation of the two column segments on either side of the splice.	0.02; 0.4 0.02; 0.4 0.05; 0.4
Bolted shear tab gravity connections	Story drift ration	DS1/DS2 DS3	**DS1**: Yielding of shear tab and elongation of bolt holes, possible crack initiation around bolt holes or at shear tab weld. Damage in field is either obscured or deemed to not warrant repair. **DS2**: Yielding of shear tab and elongation of bolt holes, possible crack initiation around bolt holes or at shear tab weld. **DS3**: Partial tearing of shear tab and possibility of bolt shear failure (6-bolt or deeper connections).	0.04; 0.4 0.04; 0.4 0.08; 0.4
Glass Type Curtain Walls	Story drift ratio	DS1 DS2	**DS1**: Glass cracking. **DS2**: Glass falls from frame.	0.0084; 0.25 0.0107; 0.35
Gypsum Wall Partitions	Story drift ratio	DS1 DS2 DS3	**DS1**: Screw pop-out, cracking of wall board, warping or cracking of tape, slight crushing of wall panel at corners. **DS2**: Moderate cracking or crushing of gypsum wall boards (typically in corners). Moderate corner gap openings, bending of boundary studs. **DS3**: Buckling of studs and tearing of tracks. Tearing or bending of top track, tearing at corners with transverse walls, large gap openings and walls displaced.	0.004; 0.45 0.011; 0.35 0.019; 0.25

presented in the earlier sections, both peak and RMS variations of accelerations are equally important statistics of design criteria. Figs. 22 and 23 show the peak accelerations in across-wind and along-wind directions and Fig. 24 shows the RMS variation of acceleration responses. Peak accelerations are compared with the limit states given in AIJ [84] and ASCE Pre-standard [15] by converting the wind speeds to their corresponding 1-year return wind speeds. This is because, depending on the slenderness of buildings, the dynamic response can cause perceptible accelerations at relatively low return period wind speeds. This drives the requirement to assess occupant comfort criteria at lower return period wind speeds [15]. The wind speed conversion is carried by using a factor given by Peterka and Shahid [85], as follows:

$$F_{RC} = 0.36 + 0.10\ln(12T) \tag{34}$$

where, F_{RC} is the return period factor for the continental United States and T ($\geq$1 year) is the return period of wind speed. Using equation (34), the one-year return wind speeds corresponding to the wind speeds 31–67 m/s, the corresponding peak accelerations with and without self-excited forces and their corresponding highest percentages of perception to the building's fundamental frequency (0.22 Hz) are given in Table 7 [84]. The accelerations in the along-wind and across-wind directions are shown in the table. From the table it can be seen that the % perception changes with the addition of SEF. For the wind speeds below cross over wind speed, the addition of SEF causes a decrease in % perception in the along-wind direction. However, it causes a much higher % perception in the across-wind direction and hence negatively impacts the residents in the overall occupant comfort. As per the limit states set by AIJ [84], the table shows 70% perception for a wind speed of 54 m/s and 90% perception for higher wind speeds in the along-wind direction. The across-wind accelerations are much higher and shows 90% perception for 36 m/s wind speeds and higher. Hence, it is clear that incorporating SEF into design loads affects the occupant comfort significantly. The percentages reported for the building are also very high and hence shows close attention should be paid to occupant comfort criteria and the building damping and design parameters should be improved to meet the comfort standards.

As per the recommendations of Irwin [80] which served as the basis for the development of ISO 6897, not more than 12% of the occupants should perceive motion due to wind speeds with a return period of 1 year. B-44 shows more than 70% of occupants perceiving motion based on the limit states given by AIJ [84] and hence requires to be designed specifically to satisfy occupant comfort requirements. As per the limit states given by ASCE Pre-standard [15], the occupant comfort limits are also crossed at low wind speeds in the across-wind direction with the effects of self-excited forces. The same can be inferred based on the threshold limits set by Goto [62]. The RMS accelerations given in Fig. 23 can be used to compare the limit states given by ISO 6897. The limiting RMS acceleration for a general-purpose building with a frequency of 0.22 Hz is 0.048 m/s^2. RMS accelerations for wind speeds over the design wind speeds are above this limit with the addition of self-excited forces. The criteria based on RMS accelerations proves to be satisfactory for the building. However, the building showed significant occupant discomfort for criteria based on peak accelerations and hence can be concluded that both peak and RMS accelerations should be considered for occupant comfort building design.

6.2. Case study 2: B-60

The analyses and response evaluation conducted on B-44 was repeated for a 60-story building to capture the effects of higher turbulence in higher floors. The results presented in Fig. 24 show the displacements and accelerations at the top of the building under the action of wind speeds varying between 18 m/s and 67 m/s. The figure also shows the RMS variation of accelerations with varying wind speeds. The displacements and accelerations have been normalized (ratio of peak response at any wind speed to the peak response at highest wind speed (58 m/s)) to make meaningful comparisons between the buildings due to their difference in heights. Fig. 24(a) and (b) show displacements in along-wind and across-wind directions, respectively. The figures show a significant increase in response over 45 m/s with the addition of *SEF* in B-44. However, B-60 shows a significant increase at a much lower wind speed at $\sim$ 35 m/s. It can also be seen that the difference in displacements between B-44 and B-60 are much lower without *SEF* and the slopes increase significantly for both buildings beyond 45 m/s showing signs of nonlinearity in response. The divergence in response from B-44 is significant for B-60 with the addition of *SEF* signaling earlier onset of nonlinearity. Fig. 24(c) and (d) shows the peak acceleration comparisons in the along-wind and across-wind directions. The figures clearly show very high acceleration responses with *SEF* on B-60 whereas the increase in accelerations is not significant for B-44 with the addition of *SEF*. The early onset of nonlinearity at lower wind speeds for B-60 is also observed in the acceleration responses shown. The RMS accelerations presented in Fig. 24(e) shows a lower divergence in responses indicating that the peaks presented occur rarely and for very short durations of loading.

The Peak and RMS accelerations given in the figures are compared with the limit states given by AIJ [84] and ISO 6897 [82], respectively. The fundamental frequency of the building is 0.13 Hz and the

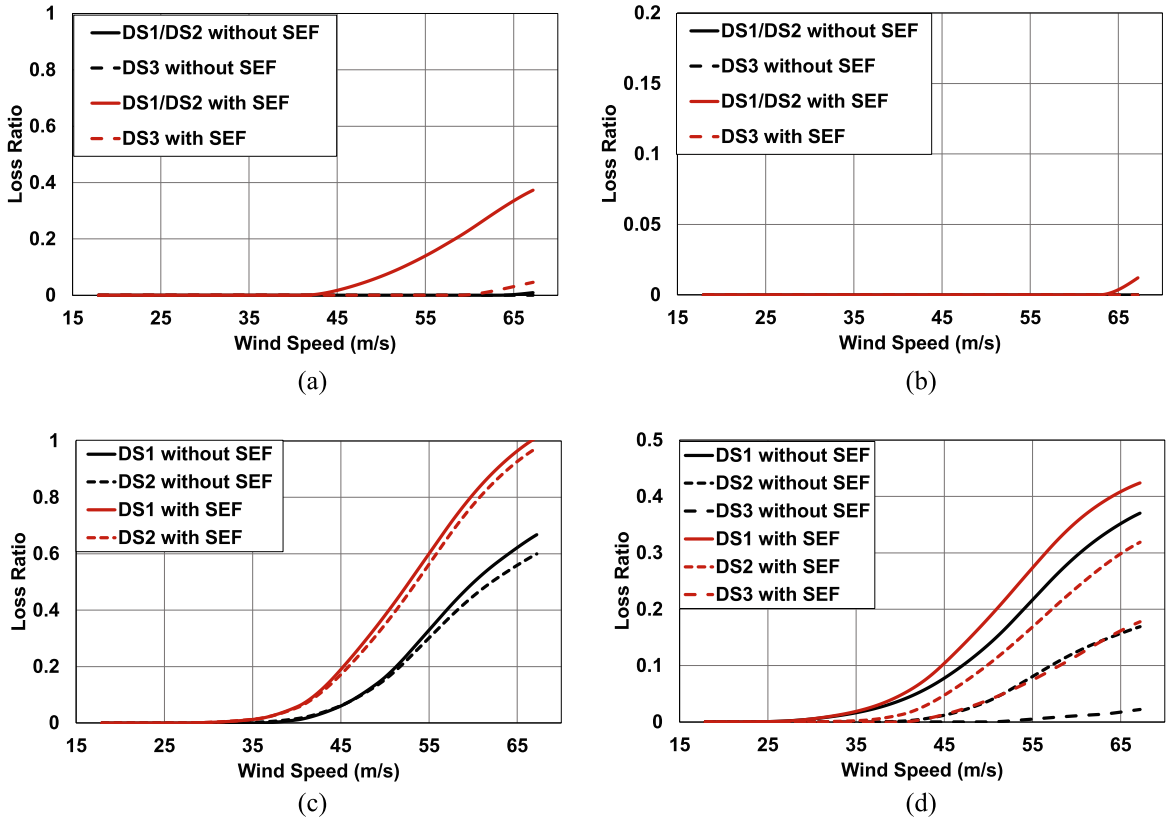

Fig. 25. Loss ratios for structural and non-structural components of B-44 building for various wind speeds (a) welded column splices, (b) bolted shear tab gravity connections, (c) glass type curtain walls and (d) gypsum partition walls.

corresponding level of human perception based on AIJ [84] limit states is given in Table 8. The table shows a high % perception for across-wind accelerations for all wind speeds without *SEF*. This indicates that the building needs to be specifically designed for occupant comfort criteria in addition to the standard strength and serviceability criteria used in the orig̣nal design. Addition of *SEF* increases the acceleration . This means even if the building is designed for occupant comfort, the residents could still experience discomfort unless the *SEF* are considered in the analysis process. The percentage of perception is also greater than 12% as per recommendations given by Irwin for all the wind speeds reported further indicating occupant specific design is to be considered. Along with the insufficiency in design criteria of the building excluding s*SEF*, this also calls into question the need for revised design standards when it comes to human comfort criteria. The figures also show peak accelerations with and without *SEF* are shown to be significantly different for the wind speeds reported. B-60 responses are also seen to be much higher than B-44 which is expected.

6.3. Loss assessment

The structural response and damage observed from the nonlinear time-history analysis can be used to quantify the losses associated with structural and non-structural damage. FEMA has developed methods to correlate the response of the buildings under seismic hazards to the structural and non-structural damage and its ramifications in terms of cost to damage. The methodology has been adopted in this study to explore the structural damage due to wind events of various recurrence intervals. The response parameters are compared with the limiting threshold specified by FEMA to categorize the structural components into different levels of damage states (*DS*) upon the action of wind loads. From the extensive FEMA database, a group of structural and non-structural components (i.e., Fragility groups (*FG*) given by FEMA) are chosen for the loss analysis in this study. The details of the *FG*s along with their limit states of damage are given in Table 9. The probability of exceedance of *DS* is then calculated from the median, dispersion, and distribution functions. The exceedance probability may then be used to evaluate the losses due to repair or replacement of the component. The cost of repair/replacement for the fragility groups are also given by FEMA and can be obtained from the FEMA P-58 [86] database. In this study, the loss ratio is the parameter used, which is the ratio of repair to replacement cost. So, if the loss ratio is reported as 1, it means the cost of repair is either equal to or greater than the cost of replacement and that the component must be replaced. The probability of exceedance corresponding to the highest story drift ratio is obtained from the curves. The loss analysis is presented for the 44-story building with and without *SEF*. The loss ratios for the *FG*s chosen in the study are given in Fig. 25(a) to 25(d). From the figures, the losses are much higher for the structural and non-structural components with the addition of self-excited forces consistent with the previous observations of drift ratios. The loss ratio is nearly zero for the structural connections without the self-excited forces which can be seen from Fig. 25(a) and (b). The loss ratios are also significant low for wind speeds below 45 m/s which is close to the design wind speed of 58 m/s. This shows that regularly occurring wind actions on buildings with shorter return periods, although causes higher discomfort to occupants does not lead to significant structural/non-structural damages or losses.

7. Conclusions

- A mathematical model to characterize the interaction of wind-building is developed.
- The load model captures the self-excited loads in its response analysis corresponding to the three-degree-of-freedom response motions of the building in along-wind, across-wind, and torsional directions.

- Interaction of post-elastic response of the structure in extreme conditions and the wind loads has been characterized through a looped structural analysis module.
- The provided approach allows for establishment of performance-based design techniques for wind-excited structure capturing the true nature of the interaction parameter.

CRediT authorship contribution statement

Smrithi Preetha Hareendran: Data curation, Formal analysis, Investigation, Validation, Visualization, Writing – original draft. **Alice Alipour:** Conceptualization, Funding acquisition, Investigation, Methodology, Project administration, Resources, Supervision, Writing – review & editing. **Behrouz Shafei:** Investigation, Methodology, Resources, Supervision, Writing – review & editing. **Partha Sarkar:** Investigation, Methodology, Resources, Supervision, Writing – review & editing.

Declaration of Competing Interest

The authors declare the following financial interests/personal relationships which may be considered as potential competing interests: Alice Alipour reports financial support was provided by National Science Foundation Grants # 1826356, 1827774, and 2214039.

Data availability

Data will be made available on request.

References

[1] Paulotto C, Ciampoli M, and Augusti G, Some proposals for a first step towards a Performance Based Wind Engineering, 2004, Proc. International Forum of Engineering Decision Making; First Forum.
[2] Sarkar PP, Caracoglia L, Haan FL, Sato H, and Murakoshi J, Comparative and sensitivity study of flutter derivatives of selected bridge deck sections, Part 1: Analysis of inter-laboratory experimental data, 2009, Engineering Structures; 31.
[3] Seo DW, Caracoglia L. Estimation of torsional-flutter probability in flexible bridges considering randomness in flutter derivatives. Eng Struct 2011;33.
[4] Seo DW, Caracoglia L. Estimating life-cycle monetary losses due to wind hazards: Fragility analysis of long-span bridges. Eng Struct 2013;56.
[5] Spence SMJ, Bernardini E, and Kareem A, A First Step towards a General Methodology for the Performance-Based Design of Wind-Excited Structures, 2015, Structures Congress.
[6] Ciampoli M, and Petrini F, Performance-based Aeolian risk assessment and reduction for tall buildings, 2012, Probabilistic Engineering Mechanics.
[7] Petrini F, and Ciampoli M, Performance-based wind design of tall buildings, 2012, Structure and Infrastructure Engineering, 8.
[8] Petrini F, Ciampoli M, and Augusti G, A probabilistic framework for Performance-Based Wind Engineering, 2009, Proceedings of Fifth European and African conference on Wind Engineering, Italy.
[9] Micheli L, Hong J, Laflamme S, and Alipour A, Surrogate models for high performance control systems in wind-excited tall buildings, 2020, Applied Soft Computing Journal, 90.
[10] Micheli L, Cao L, Gong Y, Cancelli A, Laflamme S, Alipour A. Probabilistic performance-based design for high performance control systems. Active and Passive smart Structures and Integrated Systems 2017;10164:555–68.
[11] Micheli L, Alipour A, and Laflamme, S, Multiple-surrogate models for probabilistic performance assessment of wind-excited tall buildings under uncertainties, 2020, ASCE-ASME J. Risk Uncertain. Eng. Syst. Part A Civ. Eng., 6.
[12] Micheli L, Alipour A, Laflamme S. Data-Driven Risk-Based Assessment of Wind-Excited Tall Buildings. In: Proc. Structures Congress 2019: Blast, Impact Loading. and Research and Education; 2019. p. 373–84.
[13] Micheli L, Alipour A, and Laflamme S, Performance-Based Design for Wind-Excited Tall Buildings Equipped with High Performance Control Systems, 2018, Structures Congress 2018: Buildings and Disaster Management.
[14] Micheli L, Cao l, Laflamme S, and Alipour A, Life-Cycle Cost Evaluation Strategy for High-Performance Control Systems under Uncertainties, 2020, Journal of Engineering Mechanics, 146.
[15] Prestandard for Performance Based Wind Design 2019.
[16] Buildings and Other Structures 2016.
[17] Hareendran SP, Alipour A, Shafei B and Sarkar P, Performance Based Wind Design of Tall Buildings Considering the Nonlinearity in Building Response, 2022, Journal of Structural Engineering, 148.
[18] Ouyang Z, and Spence SMJ, A performance-based wind engineering framework for envelope systems of engineered buildings subject to directional wind and rain hazards, 2020, Journal of Structural Engineering, 146 (5): 04020049. 10.1061/(ASCE)ST.1943-541X.0002568.
[19] Ouyang Z, and Spence SMJ, Performance-based wind-induced structural and envelope damage assessment of engineered buildings through nonlinear dynamic analysis, 2021, Journal of Wind Engineering and Industrial Aerodynamics, 208 (1): 104452. 10.1016/j.jweia.2020.104452.
[20] Ouyang Z, and Spence SMJ, A performance-based wind engineering framework for engineered building systems subject to hurricanes, 2021, Frontiers in Built Environment, 133.
[21] Bezabeh MA, Bitsuamlak GT, and Tesfamariam SX, Non-linear dynamic response of single-degree-of-freedom systems subjected to along-wind loads. I: Parametric study, 2021, Journal of Structural Engineering, 147 (11):04021177.10.1061/(ASCE)ST.1943-541X.0003125.
[22] Bezabeh MA, Bitsuamlak GT, and Tesfamariam SX, Non-linear dynamic response of single-degree-of-freedom systems subjected to along-wind loads. II: Implications for structural reliability, Journal of Structural Engineering, 147 (11): 04021178.10.1061/(ASCE)ST.1943-541X.0003124.
[23] Huang J, and Chen X, Inelastic performance of high-rise buildings to simultaneous actions of along wind and cross wind loads, 2022, Journal of Structural Engineering, 148 (2): 04021258. 10.1061/(ASCE)ST.1943-541X.0003236.
[24] Arunachalam S, Spence SMJ. Reliability-Based Collapse Assessment of Wind-Excited Steel Structures within Performance-Based Wind Engineering. J Struct Eng 2022;148(9):04022132.
[25] Chuang WC, Spence SMJ, A,. framework for the efficient reliability assessment of inelastic wind excited structures at dynamic shakedown. J Wind Eng Ind Aerodyn 2022;220:104834. https://doi.org/10.1016/j.jweia.2021.104834.
[26] Cui W, and Caracoglia L, Performance-based wind engineering of tall buildings examining life-cycle downtime and multisource wind damage, 2020, Journal of Structural Engineering, 146 (1): 04019179. 10.1061/(ASCE)ST.1943-541X.0002479.
[27] Feng C, Chen X. Inelastic responses of wind-excited tall buildings: Improved estimation and understanding by statistical linearization approaches. Eng Struct 2018;159(Mar):141–54. https://doi.org/10.1016/j.engstruct.2017.12.041.
[28] Judd JP, Windstorm resilience of a 10-story steel frame office building, 2018, ASCE-ASME J. Risk Uncertainty Eng. Syst. Part A: Civ. Eng. 4 (3): 04018020. 10.1061/AJRUA6.0000971.
[29] Ghaffary A, and Moustafa MM, Performance-based assessment and structural response of 20-story SAC building under wind hazards through collapse, 2021, Journal of Structural Engineering, 147 (3): 04020346. 10.1061/(ASCE)ST.1943-541X.0002911.
[30] Bernardini E, Spence SMJ, Kwon DK, and Kareem A, Performance-based design of high-rise buildings for occupant comfort, 2015, Journal of Structural Engineering, 141.
[31] Zheng X, Li H, Li C. Damage probability analysis of a high-rise building against wind excitation with recorded field data and direction effect. J Wind Eng Ind Aerodyn 2019;184:10–22.
[32] Ierimonti L, Venanzi I, Caracoglia L, and Materazzi AL, Costbased design of nonstructural elements for tall buildings under extreme wind environments, 2019, Journal of Aerospace Engineering, 32 (3).
[33] Mohammadi A, Azizinamini A, Griffis L, and Irwin P, Performance assessment of an existing 47-story high-rise building under extreme wind loads, 2019, Journal of Structural Engineering, 145 (1): 04018232. 10.1061/(ASCE)ST.1943-541X.0002239.
[34] Hou F, and Sarkar PP, A time-domain method for predicting wind-induced buffeting response of tall buildings, 2018, Journal of Wind Engineering and Industrial Aerodynamics, 182.
[35] Jafari M, Alipour A. Methodologies to mitigate wind-induced vibration of tall buildings: A state-of-the-art review. J Build Eng 2021;33:1–25. 101582.
[36] Hou F, Sarkar PP, Alipour A. A novel mechanism-smart morphing façade system-to mitigate wind-induced vibration of tall buildings. Eng Struct 2022;275. 115152.
[37] Jafari M, Alipour A. Review of approaches, opportunities, and future directions for improving aerodynamics of tall buildings with smart facades. J Sustain Cities Soc 2021;72:1–20. 102979.
[38] Abdelaziz K, Alipour A, Hobeck J. A smart façade system controller for optimized wind-induced vibration mitigation in tall buildings. J Wind Eng Ind Aerodyn 2021;212:1–10. 104601.
[39] Jafari M, Alipour A. Aerodynamic shape optimization of rectangular and elliptical double-skin façades to mitigate wind-induced effects on tall buildings. J Wind Eng Ind Aerodyn 2021;213:1–25. 104586.
[40] Hou F, Sarkar PP, Time-domain Model for Prediction of Generalized 3DOF Buffeting Response of Tall Buildings using 2D Aerodynamic Sectional Properties, 2021, Engineering Structures, 111847.
[41] Wilde K, Fujino Y, Masukawa J. Time Domain Modeling of Bridge Deck Flutter, Journal of Structural Mechanics and Earthquake. Engineering 1996;13.
[42] Chen BX, Matsumoto M, Kareem A. Aerodynamic Coupling Effects on Flutter and Buffeting of Bridges. J Eng Mech 2000;126.
[43] Cao B, Sarkar PP. Identification of Rational Functions by Forced Vibration Method for Time-Domain Analysis of Flexible Structures. The fifth International Symposium on Computational Wind Engineering. 2010.
[44] Chowdhury AG, and Sarkar PP, A new technique for identification of eighteen flutter derivatives using a three-degree-of-freedom section model, 2003, Engineering Structures, 25.
[45] Chowdhury AG, and Sarkar PP, Experimental identification of rational function coefficients for time-domain flutter analysis, 2005, Engineering Structures, 27.

[46] Chowdhury AG, Identification of frequency domain and time domain aeroelastic parameters for flutter analysis of flexible structures, 2004, Dissertation from Iowa State University.
[47] Mishra SS, Kumar K, and Krishna P, Multimode flutter of long-span cable-stayed bridge based on 18 experimental aeroelastic derivatives, 2008, Journal of Wind Engineering and Industrial Aerodynamics, 96.
[48] Scanlan RH, The Action of Flexible Bridges under Wind, I: Flutter Theory, 1978, Journal of Sound and Vibration, 60.
[49] Sauder HS, and Sarkar PP, A 3DOF forced vibration system for time-domain aeroelastic parameter identification, 2017, Wind and Structures- An International Journal, 24.
[50] AISC (American Institute of Steel Construction), Specification for Structural Steel Buildings (ANSI/AISC-360, 2016.
[51] CSI, SAP2000 Integrated Software for Structural Analysis and Design, Computers and Structures Inc., Berkeley, California.
[52] McKenna F, Fenves GL, and Scott MH, Open System for Earthquake Engineering Simulation, 2000, University of California, Berkeley.
[53] Applied Technology Council (ATC), Modeling and Acceptance Criteria for Seismic Design and Analysis of Tall Buildings, 2010, Redwood city, California.
[54] Deodatis G. Simulation of Ergodic Multivariate Stochastic Processes. J Eng Mech 1996;122:778–87.
[55] Kaimal JC, Wyngaard JC, Izumi Y and Coté OR, Spectral characteristics of surface-layer turbulence, 1972, Quarterly Journal of The Royal Meteorological Society, 10.1002/qj.49709841707.
[56] Hareendran SP, Alipour A, Prediction of nonlinear structural response under wind loads using deep learning techniques, Appl Soft Comput 129, 109424.
[57] Saini DS, Alipour A, Shafei B. Database-Assisted Design of High-Rise Steel Structures Using ETABS Software; 2022, 10.6028/NIST.GCR.22-035.
[58] Tsai L-W, Alipour A. Physics-informed long short-term memory networks for response prediction of a wind-excited flexible structure. Eng Struct 2023;275:114968.
[59] Dikshit, S. an dAlipour, A."A moment-matching method for fragility analysis of transmission towers under straight line winds", Reliability Engineering an dsystem Safety, Volume 236, August 2023, 109241.
[60] Hansen RJ, Reed JW, and Vanmarcke EH, Human Response to Wind-Induced Motion of Buildings, 1973 Journal of the Structural Division, 99.
[61] Melbourne WH, and Palmer TR, Accelerations and comfort criteria for buildings undergoing complex motions, 1992, Journal of Wind Engineering and Industrial Aerodynamics.
[62] Goto T. Studies on Wind-Induced Motion of Tall Buildings based on Occupants Reactions. J Wind Eng Ind Aerodyn 1983;13.
[63] Lee BE, The Perception of The Wind-Induced Vibration of a Tall Building: A Personal Viewpoint, 1983, Journal of Wind Engineering and Industrial Aerodynamics, 12.
[64] Chang FK, Wind and Movement in Tall Buildings, 1967, Civil Engineering, ASCE, 37.8.
[65] Denoon RO, Letchford CW, Kwok KCS, and Morrison DL, Field Measurements of Human Reaction to wind-induced building motion, 1999, Wind Engineering into the 21st Century.
[66] Denoon RO, Roberts RD, Letchford CW, Dphil BE, and Kwok KCS, Field Experiments to Investigate Occupant Perception and Tolerance of Wind-Induced Building Motion, 2000, Research Report No R803.
[67] Correa TK. Validating Wind-Induced Response of Tall Buildings: Synopsis of the Chicago Full-Scale Monitoring Program. J Struct Eng 2006;132.
[68] Correa TK, Pirnia JD. Pseudo-Full scale evaluation of Occupant Comfort in Tall Buildings. Proceedings of 11th Americas conference on Wind Engineering. 2009.
[69] Lamb S, Kwok KCS, and Walton D, Occupant comfort in wind-excited tall buildings: Motion sickness, compensatory behaviors and complaint, 2013, Journal of Wind Engineering and Industrial Aerodynamics, 119.
[70] Golding JF, Predicting individual differences in motion sickness susceptibility by questionnaire, 2006, Personality and Individual Differences, 41.
[71] Irwin AW, Perception, Comfort and Performance criteria for Human Beings Exposed to Whole body pure yaw vibration and vibration containing yaw and translational components, 1981, Journal of Sound and Vibration.
[72] Michaels MN, Kwok KCS, and Tung YK, Exploratory analyses and modelling of parameters influencing occupant behavior due to low-frequency random building motion, 2013, Journal of Wind Engineering and Industrial Aerodynamics, 115.
[73] Goto T, An Experimental Study on the Relationship Between Motion and Habitability in a Tall Residential Building, 1990, Proceedings of Tall Buildings: 2000 and Beyond, Fourth World Congress.
[74] Kanda J, Probabilistic perception limits of low-frequency horizontal motions, 1990, Conference on Serviceability of Steel and Composite Structures.
[75] Kanda J, Probabilistic criteria for human perception of low-frequency horizontal motions, 1988, Symposium/Workshop on Serviceability of Buildings (Movements, Deformations, Vibrations).
[76] Shioya K. Human Perception Thresholds of Horizontal Motion. Structural Seviceability of Buildings; 1993.
[77] Tamura Y. Evaluation perception of wind-induced vibration in buildings. Struct Build 2006;159.
[78] Morris RC, Dennis I, Tomlinson RW, Clarke A. Vibration in Tall buildings. Plymouth Polytechnic, United Kingdom: B.R.E. Contract Report; 1980.
[79] Bouncer TH, Morris RC, Tomlinson RW, Perception Threshold Responses to induced Low-Frequency Motion of Tall Buildings, 1980, Final Report S. R. C. Contract No. GR/B 20938, Plymouth Polytechnic, United Kingdom.
[80] Irwin AW. Human Reactions to Oscillations of Buildings: Acceptable Limits. Build International; 1975.
[81] Irwin AW, Human Response to Dynamic Motion of Structures, The Structural Engineer, 56A(9); 1978.
[82] ISO (International Organization of Standardization) 6897, Guidelines for the evaluation of the response of occupants of fixed structures, especially buildings and off-shore structures, to low-frequency horizontal motion (0.063-1 Hz); 1984, https://www.iso.org/obp/ui/#iso:std:13419:en.
[83] Melbourne WH, Cheung JCK, Designing for serviceable accelerations in Tall Buildings. Proceedings of Fourth International Conference on Tall Buildings, Hong Kong and Shanghai; 1988.
[84] AIJ (Architectural Institute of Japan) Recommendations, Guidelines for the evaluation of habitability to building vibration, Tokyo, Japan; 2004.
[85] Peterka JA, Shahid S. Design Gust Wind Speeds in The United States. J Struct Eng 1998.
[86] FEMA-P-58, Seismic Performance Assessment of Buildings, Applied Technology Council, Redwood City, CA, 3; 2018.